Multiuser Detection for Transmit-Only Active RFID

by

Dana Hoffmann

B.Sc., Electrical Engineering, Technion - Israel Institute of Technology, 2004

B.A., Physics, Technion - Israel Institute of Technology, 2004

A THESIS SUBMITTED IN PARTIAL FULFILLMENT
OF THE REQUIREMENTS FOR THE DEGREE OF

Master of Applied Science

in

THE FACULTY OF GRADUATE STUDIES

(Electrical and Computer Engineering)

The University Of British Columbia

(Vancouver)

December 2011

Abstract

One of the biggest challenges in Radio Frequency Identification (RFID) systems is mitigating tag collisions. Most systems tackle this problem using Medium Access Control layer solutions. Unfortunately, these solutions are not applicable to systems with transmit-only tags, since the tags cannot detect collisions. This thesis introduces a novel reader design that employs multiuser detection techniques to jointly detect data from colliding packets in such systems. We propose a physical layer solution that exploits signal structure to mitigate tag collisions. Since the RFID tags generate their own clock using inexpensive hardware, this framework poses some unique challenges. We present methods for collision detection, synchronization, and channel estimation, as well as demodulation of the colliding signals. We show simulation results that demonstrate the gains in performance obtained using the proposed solution.

Table of Contents

List of Tables

List of Figures

Glossary

The following are abbreviations and acronyms used in this thesis.

RFID	Radio Frequency Identification
PHY	Physical Layer
ID	Identification
MAC	Medium Access Control
MUD	Multiuser Detection
SUD	Single User Detection
MSK	Minimum Shift Keying
GMSK	Gaussian Minimum Shift Keying
OOK	On Off Keying
AWGN	Additive White Gaussian Noise
BER	Bit Error Rate
PER	Packet Error Rate

BPSK	Binary Phase Shift Keying
ISI	Inter Symbol Interference
MFB	Matched Filter Bound
MSE	Mean Square Error
MMSE	Minimum Mean Square Error
ZF	Zero Forcing
SNR	Signal to Noise Ratio
SIR	Signal to Interference Ratio
WL	Widely Linear
MIC	Mono Interference Cancellation
MIMO	Multiple-Input Multiple-Output
LS	Least Squares
LMS	Least Mean Squares
CDF	Cumulative Distribution Function

Acknowledgments

I owe my deepest gratitude to my supervisor, Prof. Lutz Lampe, for his continued patience and support. I could not have completed this thesis without his help and enthusiasm. Special thanks and appreciation to Dr. Sara Bavarian for all her help and encouragement.

I would also like to thank my colleagues in the lab for their friendship and encouragement. Many thanks go to my excellent support network: my family in Israel for their love and support; my friends in Vancouver for all the awesome trips, dinners and game nights; and last but not least, my husband Ron, for being my best friend and partner, and for doing a great job taking care of me so I could finish writing this thesis. Thank you all for making graduate school such an amazing adventure.

Chapter 1

Introduction

Radio Frequency Identification (RFID) is a wireless communications technology used for identifying, tracking and locating a physical object. RFID has applications in many different industries such as inventory control, tracking people and assets (e.g. mobile medical equipment, hospital patients and personnel), electronic toll collection, and access control. Generally, an RFID system is composed of multiple identifying tags that are attached to the objects, and readers that collect data from the tags. Often there is also a central processing unit that gathers and processes data from the readers. There can typically be thousands of tags in the range of a single reader, e.g. in a warehouse application [1]. A typical system is illustrated in Figure 1.1.

RFID tags can generally be classified as active or passive. Passive tags harvest energy from the signal they receive from the reader and use it to transmit their data, which limits their range. Active tags contain a battery and generate their own radio signal, providing better range and reliability. They are typically more expensive than passive tags, and have a limited battery life. However, this type of system has

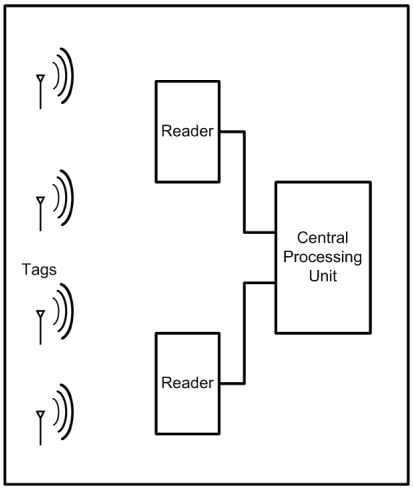

Figure 1.1: A typical RFID system

an advantage in applications that require monitoring and data logging, because the tags can remain operational even when they are out of reader range.

Our research is based on the system model introduced by the IEEE 802.15.4f task group, which defines a new wireless Physical Layer (PHY) standard for active RFID systems [2]. Their aim is to define a global standard that will enable low cost, low power consumption and reliable PHY layer interface for active RFID. The standard proposal includes three PHY variants: one ultra wideband and two narrowband schemes operating at 2.4 GHz and 433 MHz. To allow better flexibility and support appropriate solutions for a wider set of applications, the proposal introduces an optional simplex mode with transmit-only tags that benefits from low power con-

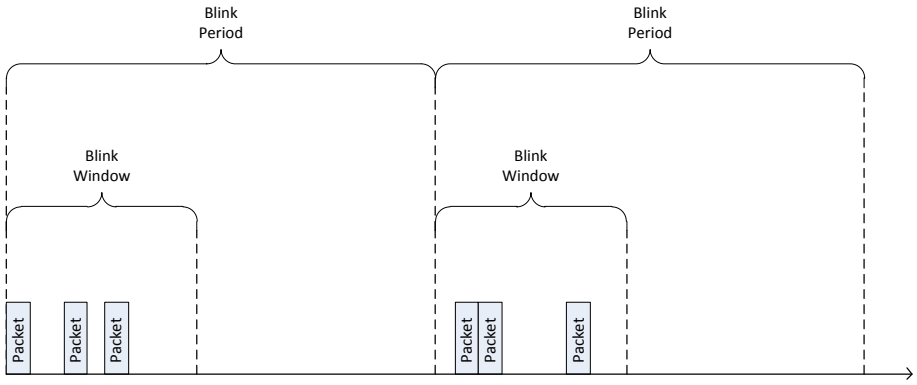

Figure 1.2: Illustration of the Double-P-Aloha collision avoidance mechanism. A transmit-only RFID tag periodically transmits its packets every blink period. This scheme defines a blink window at the start of each blink period, in which the tag transmits several redundant copies of the packets.

sumption and simple tag design. In this mode each tag periodically transmits its Identification (ID) packet, and the communication is one-way and asynchronous. This type of system offers interesting challenges, and is the focus of our research. We concentrate on the narrowband transmission scheme [3], which employs Minimum Shift Keying (MSK) modulation.

A major challenge in RFID systems is tag collisions, which occur when a reader receives transmissions from multiple tags simultaneously. Most of the work undertaken to mitigate this problem has assumed that colliding packets cannot be detected and focused on anti-collision protocols in the Medium Access Control (MAC) layer, using protocols such as Slotted Aloha and Binary Splitting [4]. These MAC-based collision mitigation solutions are based on the tags retransmitting their packets when collisions are detected. Since they require the tags to either

sense the channel and detect the collisions themselves, or receive an acknowledgment from the reader, they are not feasible in the transmit-only scheme. As part of the standardization effort for active RFID, one possible mechanism was proposed that addresses this problem. The suggested solution is a variation of pure Aloha called Double-P-Aloha [3], illustrated in Figure 1.2. Each transmit-only tag transmits its ID packet every blink period, and since their clocks are generated independently the starting times of the blink periods vary across tags. The collision avoidance mechanism offers another layer of redundancy and randomization, by defining a blink window at the beginning of each blink period, and having each tag transmit redundant packets at randomized time instances within that window. This algorithm increases the probability of the reader successfully receiving one of the redundant packets, at the cost of increased traffic and power consumption.

In this work, we take a distinctly different approach. More specifically, we tackle the tag collision problem using a Multiuser Detection (MUD) technique in the PHY layer, where we exploit the MSK signal structure to jointly detect colliding packets. Since MSK uses a real-valued symbol constellation, the complex-valued received signal contains another degree of freedom, potentially enabling us to detect two packets simultaneously. Using multiple antennas at the receiver could further increase the number of signals we can jointly detect. While we focus on the transmit-only case, our approach is also applicable to bidirectional RFID systems. Even in cases where MAC solutions are feasible, our approach shifts the complexity from the tags to the readers, enabling a cheaper, more power-efficient tag design.

1.1 Organization

This thesis presents our solution for mitigating tag collisions in the PHY level for an active RFID system. Chapter 2 begins by demonstrating the potential performance improvement of our approach, using MAC-layer analysis. We then present a brief overview of relevant existing work. We introduce the signal structure that is used in the following chapters in Chapter 3. The next two chapters discuss two MUD schemes that can be used to detect data from multiple tags during a collision. Chapter 6 and Chapter 7 show our proposed channel estimation and packet acquisition algorithms. Finally, a full system overview and simulation results are given in Chapter 8.

Chapter 2

Motivation and Related Work

2.1 Motivation

MUD techniques can be used to jointly detect the data transmitted from multiple tags simultaneously, thus enabling us to extract information even in the presence of tag collisions. We start by demonstrating the potential advantage of this approach, using the properties of Aloha systems [5].

In our system model, every tag transmits its ID periodically with a blink period of T_{blink}. A collision occurs if more than one tag transmits in a window of $2T_{id}$ seconds, where T_{id} is the packet duration. Since the tags use independent clocks we can assume the starting times of the blink periods are uniformly distributed. Therefore, the probability of another packet colliding with the packet under consideration is

$$p = \frac{2T_{id}}{T_{blink}} . \tag{2.1}$$

The probability of a collision with k other tags in a system with N_{tags} tags is given

by the Binomial distribution:

$$P_k = P(k \text{ arrivals in } n \text{ trials}) = \frac{n!}{k!(n-k)!} p^k (1-p)^{n-k} , \tag{2.2}$$

with $n = N_{tags}$. If each tag retransmits every packet M times, and we make the approximation that the repetitions are independent, we get a similar expression with $n = N_{tags}M$.

When the probability p from Equation 2.1 is small, and the number of trials n is large, the Binomial distribution can be approximated by the Poisson distribution with a parameter λ:

$$\begin{aligned} P_k &= P(k \text{ arrivals in } 2T_{id} \text{ seconds}) = \frac{e^{-\lambda}\lambda^k}{k!} \\ \lambda &= np = MN_{tags}\frac{2T_{id}}{T_{blink}} . \end{aligned} \tag{2.3}$$

The probability of no collisions for a certain packet, i.e. the probability of no other packets arriving within the $2T_{id}$ window can be expressed as

$$P_0 = e^{-\lambda} . \tag{2.4}$$

Similarly, the probability of a collision with k other packets is given by P_k from Equation 2.3.

Assuming we can jointly detect the packets when up to K tags collide, the probability that a transmitted packet is successfully detected is

$$P_{packet} = \sum_{k=0}^{K-1} P_k , \tag{2.5}$$

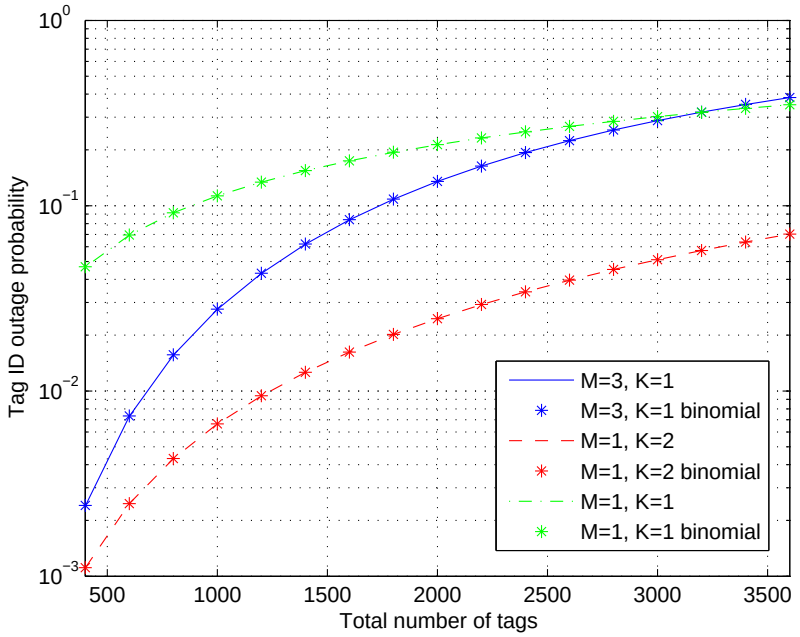

Figure 2.1: The outage probabilities in pure Aloha ($M = 1$, $K = 1$), the Double-P-Aloha scheme ($M = 3$, $K = 1$), and our proposed scheme ($M = 1$, $K = 2$). $T_{id} = 600\ \mu$sec and $T_{blink} = 10$ sec.

and the probability of a tag ID being successfully recovered at the receiver is thus

$$P_{success} = 1 - (1 - P_{packet})^M . \tag{2.6}$$

Figure 2.1 illustrates the potential performance gain assuming we can jointly detect two colliding tags, i.e. $K = 2$. It compares the outage probability of the original pure Aloha scheme, to two possible improvements: the Double-P-Aloha scheme suggested in the standardization process, in which each tag transmits its packets three times, and our alternative scheme with no repetitions that assumes that the data of two colliding packets can be extracted. In all cases we use parameters

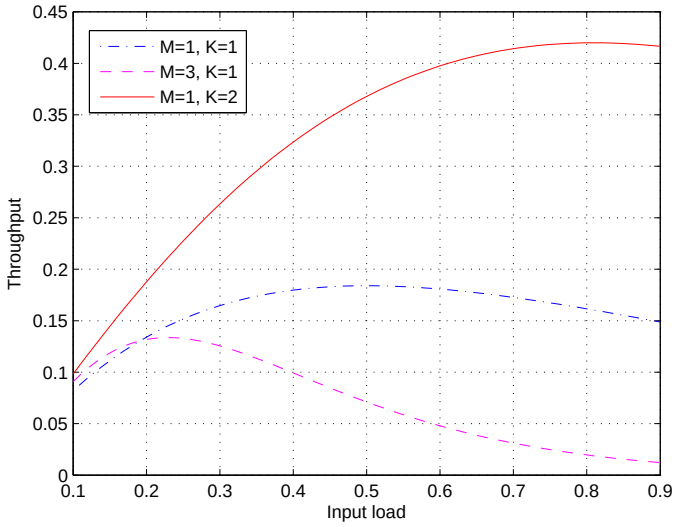

Figure 2.2: The throughput of pure Aloha ($M = 1$, $K = 1$), Double-P-Aloha ($M = 3$, $K = 1$), and joint detection ($M = 1$, $K = 2$).

specified in the standard proposal: $T_{id} = 600\,\mu$sec and $T_{blink} = 10$ sec. The apparent improvement that can be achieved by jointly detecting colliding packets means we can dramatically enhance the reliability of the system, or opt to increase tag density while keeping the same confidence level.

The joint detection also changes the optimal load of the system. The input load is defined as

$$G = \frac{N_{tags} T_{id}}{T_{blink}} , \tag{2.7}$$

and the throughput is

$$Throughput = P_{success} G , \tag{2.8}$$

so we can find the load for which we can expect the best throughput. Figure 2.2 compares the throughput curves for pure Aloha ($M = 1$, $K = 1$), double-P-Aloha

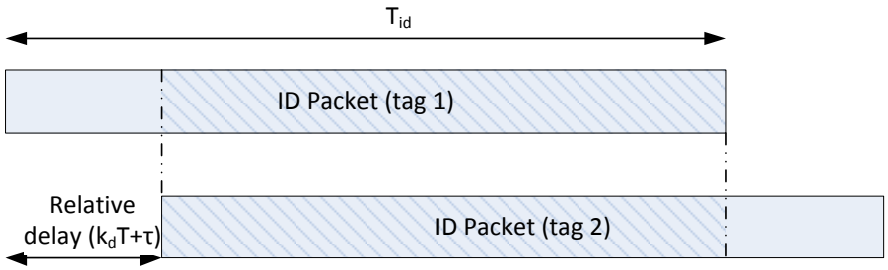

Figure 2.3: Packet collision. Joint detection is necessary within the striped region

($M = 3$, $K = 1$), and the joint detection ($M = 1$, $K = 2$) scheme. We see the optimal load in the latter case is significantly higher than for the alternatives.

The rest of this thesis will concentrate on the scenario in which two tags collide, as depicted in Figure 2.3. Our solution has to detect the arrival of the second packet, identify the relative delay and jointly detect the information bits from both packets during the overlap.

2.2 Related Work

We use MUD techniques to extract information from collided signals. By exploiting signal structure and, if available, also using multiple antennas at the receiver, these techniques enable joint detection of data transmitted from different tags. Similar methods are already employed in existing wireless systems (e.g. cellular systems) but the case of active RFID poses additional challenges. Most prior work assumes users are symbol-synchronized, or at least share the same frequency, which is not applicable in our transmit-only scheme. Since active RFID tags generate their own transmit signals using inexpensive circuitry, we have to take into account potential

frequency offsets between them.

Some relevant research has been done on the GSM cellular framework, since it employs a similar modulation scheme, Gaussian Minimum Shift Keying (GMSK). Murphy et al. [6] developed optimal and suboptimal detectors for asynchronous GMSK systems. Their solutions are based on the Laurent representation [7] of the signals and on the Viterbi algorithm. However, they assumed all users share the same frequency, an assumption which does not hold in the transmit-only scheme. Although they do handle relative delays between users, they assume these delays are only a fraction of the symbol period.

Another popular approach for detecting MSK modulation is through Widely Linear (WL) processing [8, 9]. This method is based on derotating the baseband signal, and thereby interpreting it as a form of Binary Phase Shift Keying (BPSK) modulation filtered by a complex channel. It has been shown that WL processing can be used for single antenna interference cancellation of MSK signals, by exploiting the added degree of freedom of the complex observations. Like linear filtering, WL filtering can use coefficients optimized by different criteria, namely Zero Forcing (ZF) and Minimum Mean Square Error (MMSE).

Zhang et al. [10] proposed a MUD scheme for a transmit-only RFID system using successive interference cancellation (SIC). This method is based on sequentially detecting and removing users (tags) from the received signal, starting with the stronger ones. However, their system model assumed an On Off Keying (OOK) modulation, which is simpler to detect than MSK. While they do consider varying phase differences and time delays between the tags, they do not include frequency offsets in their model.

More recently some work has been done on PHY layer collision recovery for

passive RFID systems [11–14]. Since passive tags use backscattering of the reader's signal to transmit their data, the frequency offsets and time delays they have to take into account are smaller.

Chapter 3

Signal Model

Our work is based on the transmission format specified by the IEEE 802.15.4f active RFID standard proposal. Specifically, we concentrate on the narrowband 433MHz scheme. Some of its parameters are summarized in Table 3.1. Each

Modulation	MSK
Frequency	433MHz
Bit rate	31.25 kb/s to 250 kb/s

Table 3.1: Parameters of IEEE 802.15.4f narrowband 433MHz scheme

packet includes a known header, starting with a 32-bit preamble of alternating zeros and ones, followed by a 2-byte start-of-frame delimiter with the format "01001001-10001111".

This chapter introduces the signal model used to describe the physical layer of the IEEE 802.15.4f narrowband mode. In Section 3.1 we derive the structure of a single MSK signal. Section 3.2 includes our assumptions regarding the wireless channel, and in Section 3.3 we present the signal model during a collision.

3.1 MSK Signals

The baseband equivalent representation of an MSK signal can be expressed as [9, 15]

$$s(t) = \sum_n j^n b_p[n] f(t - nT) \,, \tag{3.1}$$

where $j = \sqrt{-1}$, $b_p[n] \in \pm 1$ are the data symbols transmitted by user p, T is the symbol interval, and $f(t)$ is the pulse shape given by

$$f(t) = \begin{cases} \frac{1}{\sqrt{T}} \sin\left(\frac{\pi t}{2T}\right) & 0 \le t \le 2T \\ 0 & \text{elsewhere} \end{cases} . \tag{3.2}$$

By derotating the signal at the receiver, the useful part of the received signal can be treated as a BPSK signal with a complex pulse shaping function:

$$s_d(t) = j^{-\frac{t}{T}} s(t) = \sum_n j^{-\frac{t-nT}{T}} b_p[n] f(t - nT) = \sum_n b_p[n] f_d(t - nT) \,, \tag{3.3}$$

where $f_d(t)$ is defined as

$$f_d(t) = j^{-t} f(t) \,. \tag{3.4}$$

The derotation operation can also be performed in the digital domain with the same outcome. After matched filtering with the filter $f(-t)$, sampling with a rate $\frac{1}{T_s} = \frac{S}{T}$ (where S is the oversampling ratio), and derotating the output we get the discrete-

time signal

$$\begin{aligned} y^{(l)}[k] &= j^{-k-l/S}\, s(t) * f(-t)\big|_{t=kT+\frac{l}{S}T} \\ &= j^{-k-l/S} \sum_n b_p[n] j^n \int_{-\infty}^{\infty} f(\tilde{t}-nT) f(\tilde{t}-kT-lT/S) d\tilde{t} \\ &= \sum_i b_p[k-i] j^{-l/S} j^{-i} R_{ff}(iT+lT/S) = \sum_i b_p[k-i] f_o^{(l)}[i] \,, \end{aligned} \tag{3.5}$$

where $R_{ff}(t)$ is the pulse shape autocorrelation function

$$R_{ff}(t) = \int_{-\infty}^{\infty} f(\tilde{t}) f(\tilde{t}+t) d\tilde{t} \,, \tag{3.6}$$

and $f_o^{(l)}[i]$ are the discrete time complex coefficients for sampling phase l ($l = 0, \ldots, S-1$)

$$f_o^{(l)}[i] = j^{-l/S} j^{-i} R_{ff}(iT+lT/S) \ . \tag{3.7}$$

These coefficients do not include the contribution of the wireless channel. We use the derotation, matched filtering and sampling as the front-end of our proposed receiver. For the remainder of this thesis, we analyze the discrete-time signals after these operations have been performed.

Let us now look at the Additive White Gaussian Noise (AWGN) as it propagates through this front-end. The derotation itself does not change the noise properties. After matched filtering, sampling and derotation we get the following noise components:

$$\begin{aligned} n^{(l)}[k] &= j^{-k-l/S}\, n(t) * f(-t)\big|_{t=kT+\frac{l}{S}T} \\ &= j^{-k-l/S} \int_{-\infty}^{\infty} n(\tilde{t}+kT+lT/S) f(\tilde{t}) d\tilde{t} \end{aligned} \tag{3.8}$$

The discrete noise is still Gaussian, but is now coloured. The noise autocorrelation can be expressed as

$$\begin{aligned}
\Phi_{nn}^{(m)}[i] &= \mathbb{E}\left\{ n^{(l)}[k] n^{(l+m)*}[k+i] \right\} \\
&= j^{i+m/S} \mathbb{E}\left\{ \int_{-\infty}^{\infty} n(\tilde{t} + kT + lT/S) f(\tilde{t}) d\tilde{t} \right. \\
&\qquad \left. \cdot \int_{-\infty}^{\infty} n^*(\bar{t} + (k+i)T + (l+m)T/S) f(\bar{t}) d\bar{t} \right\} \qquad (3.9) \\
&= N_0 j^{i+m/S} \int_{-\infty}^{\infty} f(\tilde{t}) f(\tilde{t} - iT - mT/S) d\tilde{t} \\
&= N_0 j^{i+m/S} R_{ff}(-iT - mT/S) \,,
\end{aligned}$$

where N_0 is the AWGN variance.

3.2 Channel Model

Since we use a narrowband transmission scheme it is reasonable to consider a flat channel model. The typical packet duration specified by the standard proposal is short (600μsec), so we can also assume the channel remains constant for the entire packet. We can therefore describe the received samples as

$$r^{(l)}[k] = \alpha_p \sum_i b_p[k-i] f_o^{(l)}[i] + n^{(l)}[k] = \sum_i b_p[k-i] h^{(l)}[i] + n^{(l)}[k] \qquad (3.10)$$

where α_p is the complex gain introduced by the channel, $h^{(l)}[i] = \alpha_p f_o^{(l)}[i]$ is the overall discrete channel response, and $n^{(l)}[k]$ is the complex Gaussian noise with covariance $N_0\Sigma$.

3.3 Multiple Tags

Let us assume we are synchronized to a first user (user 1), and now consider an unsynchronized second user (user 2). When we receive an unsynchronized MSK signal [16], Equation 3.1 becomes

$$s_2(t) = \alpha e^{j(2\pi\nu t+\theta)} \sum_n j^n b_2[n] f(t-nT-\tau) \,, \tag{3.11}$$

where $b_2[n]$ are the transmitted data symbols, α is the complex gain, ν is the frequency offset, θ is the phase offset, and $-T \leq \tau \leq T$ is the timing offset. After derotation, matched filtering and sampling, the received component corresponding to $s_2(t)$ is given by

$$\begin{aligned} y_2^{(l)}[k] &= \alpha e^{j(2\pi\nu(kT+lT/S)+\theta)} \\ &\quad \cdot \sum_i b_2[k-i] j^{-l/S-i} \int_{-\infty}^{\infty} f(\tilde{t}+iT+lT/S-\tau) f(\tilde{t}) e^{j2\pi\nu\tilde{t}} d\tilde{t} \\ &= \alpha e^{j(2\pi\nu(kT+lT/S)+\theta)} \sum_i b_2[k-i] j^{-l/S-i} R_{ff}^{\nu}(iT+lT/S-\tau) \\ &= e^{j2\pi\nu(kT+lT/S)} \sum_i b_2[k-i] h_2^{(l)}[i] \,, \end{aligned} \tag{3.12}$$

where $R_{ff}^{\nu}(t)$ is the mismatched pulse shape autocorrelation function

$$R_{ff}^{\nu}(t) = \int_{-\infty}^{\infty} f(\tilde{t}) f(\tilde{t}+t) e^{j2\pi\nu\tilde{t}} d\tilde{t} \,, \tag{3.13}$$

and the complex channel coefficients are given by

$$h_2^{(l)}[i] = \alpha e^{j\theta} j^{-l/S} j^{-i} R_{ff}^{\nu}(iT+lT/S-\tau) \,. \tag{3.14}$$

When signals from both tags arrive simultaneously at the receiver, a collision occurs. Without loss of generality, we assume the receiver is synchronized with the first packet to arrive. During the overlap between the packets (illustrated in Figure 2.3) the received samples can be expressed as

$$r^{(l)}[k] = \sum_i b_1[k-i]h_1^{(l)}[i] + e^{j2\pi\nu(kT+lT/S)}\sum_i b_2[k-i]h_2^{(l)}[i] + n^{(l)}[k]\ . \qquad (3.15)$$

In the interest of clarity, in the chapters that follow we will mostly use symbol-spaced sampling ($S = 1$) and therefore omit the sampling phase index l from the notations. The same derivations can easily be generalized to the oversampled case ($S > 1$).

Chapter 4

Joint MMSE Widely Linear Detection

In this chapter we consider the case of packets from two tags arriving simultaneously, as illustrated in Figure 2.3. We study the joint data detection during the overlap between the packets. Without loss of generality, we assume the packet transmitted by user 1 arrives first. We wish to detect data sequences $b_1[k]$ and $b_2[k]$ corresponding to user 1 and user 2 respectively. We describe an estimation structure based on WL processing [8, 9]. We start with the signal model introduced in Chapter 3 and assume symbol-spaced sampling ($S = 1$). Throughout this chapter we assume the channel coefficients $h_1[k]$ and $h_2[k]$ are perfectly known. We initially ignore the frequency offset, and later treat it as a slow change of the overall channel response. Channel and frequency offset estimation will be discussed in Chapter 6 and Chapter 7 respectively.

4.1 MIMO System Model

Since the oversampling factor is $S = 1$, let us look at a simplified version of the received samples during the overlap between the packets previously given in Equation 3.15. Omitting the sampling phase index l we get

$$\begin{aligned} r[k] &= \sum_{i=0}^{L} b_1[k-i]h_1[i] + \sum_{i=0}^{L} b_2[k-i]h_2[i] + n[k] \\ &= \sum_{i=0}^{L} \begin{bmatrix} h_1[i] & h_2[i] \end{bmatrix} \begin{bmatrix} b_1[k-i] \\ b_2[k-i] \end{bmatrix} + n[k] \end{aligned} \tag{4.1}$$

The effective discrete-time channel responses $h_1[k]$ and $h_2[k]$ depend on the pulse shape, the timing offset and the complex channel gain and thus both have a finite number of non-zero coefficients L. The real data symbols $b_1[k]$ and $b_2[k]$ are the unknown quantities we wish to jointly detect. We can achieve WL processing by decomposing all complex values into their real and imaginary components. Doing so, Equation 4.1 can be written as

$$\mathbf{r}_{IQ}[k] = \sum_{i=0}^{L} \mathbf{H}_{IQ}[i]\mathbf{b}[k-i] + \mathbf{n}_{IQ}[k] \,, \tag{4.2}$$

where

$$\begin{aligned}
\mathbf{r}_{IQ}[k] &= \begin{bmatrix} \Re\{r[k]\} & \Im\{r[k]\} \end{bmatrix}^T \\
\mathbf{n}_{IQ}[k] &= \begin{bmatrix} \Re\{n[k]\} & \Im\{n[k]\} \end{bmatrix}^T \\
\mathbf{H}_{IQ}[k] &= \begin{bmatrix} \Re\{h_1[k]\} & \Re\{h_2[k]\} \\ \Im\{h_1[k]\} & \Im\{h_2[k]\} \end{bmatrix} \\
\mathbf{b}[k] &= \begin{bmatrix} b_1[k] & b_2[k] \end{bmatrix}^T
\end{aligned} \tag{4.3}$$

with $\Re\{\cdot\}$ and $\Im\{\cdot\}$ representing the real and imaginary parts respectively. We want to detect the transmitted data symbols by filtering the received samples. For that purpose we stack N consecutive instances of $\mathbf{r}_{IQ}[k]$ (where N affects the length of the WL filter we use) and define the following variables:

$$\begin{aligned}
\mathbf{H}_{IQ} &= \begin{bmatrix} \mathbf{H}_{IQ}[0] & \cdots & \mathbf{H}_{IQ}[L] & 0 & \cdots & 0 \\ 0 & \mathbf{H}_{IQ}[0] & \cdots & \mathbf{H}_{IQ}[L] & \cdots & 0 \\ \vdots & \ddots & \ddots & \ddots & \ddots & 0 \\ 0 & \cdots & 0 & \mathbf{H}_{IQ}[0] & \cdots & \mathbf{H}_{IQ}[L] \end{bmatrix} \\
\mathbf{r}_{IQ} &= \begin{bmatrix} \mathbf{r}_{IQ}^T[k] & \mathbf{r}_{IQ}^T[k-1] & \cdots & \mathbf{r}_{IQ}^T[k-N+1] \end{bmatrix}^T \\
\mathbf{n}_{IQ} &= \begin{bmatrix} \mathbf{n}_{IQ}^T[k] & \mathbf{n}_{IQ}^T[k-1] & \cdots & \mathbf{n}_{IQ}^T[k-N+1] \end{bmatrix}^T \\
\mathbf{b} &= \begin{bmatrix} \mathbf{b}[k] & \cdots & \mathbf{b}[k-L] & \cdots & \mathbf{b}[k-N-L+1] \end{bmatrix}^T
\end{aligned} \tag{4.4}$$

where $\mathbf{H}_{IQ}$ is the $2NS \times 2(L+N)$ convolution matrix of real and imaginary channel coefficients for both users, $\mathbf{r}_{IQ}$ is a vector of the $2NS$ received samples in their real-

imaginary form, and $\mathbf{b}$ is the vector of the $2(N+L)$ real data symbols. $\mathbf{n}_{IQ}$ is a vector of the Gaussian noise samples $\mathbf{n}_{IQ}[k]$, whose covariance matrix we denote as $\frac{N_0}{2}\Sigma$. This leads to a real-valued Multiple-Input Multiple-Output (MIMO) matrix representation of our system:

$$\mathbf{r}_{IQ} = \mathbf{H}_{IQ}\mathbf{b} + \mathbf{n}_{IQ} \, . \tag{4.5}$$

With this representation, the original WL problem is transformed into an equivalent linear system. We wish to perform symbol-by-symbol linear detection of the symbols transmitted by both tags. This can be achieved by applying two $2NS$ real-valued filters $\mathbf{w}_p$ ($p = 1,2$) to the observation vector, such that the Mean Square Error (MSE) with respect to the transmitted symbols of user p is minimized. The MSE is given by

$$\mathrm{MSE}_p = \mathbb{E}\left\{ \|d_p - b_p[k-k_p]\|^2 \right\} \, , \tag{4.6}$$

where $d_p = \mathbf{w}_p^T \mathbf{r}_{IQ}$ is the decision variable for user p and k_p is the decision delay. The latter is another system parameter that can be chosen such that MSE_p is minimized. The optimized MMSE coefficients of the filter $\mathbf{w}$ are given by [17]

$$\mathbf{w} = \left(\mathbf{H}_{IQ}{\mathbf{H}_{IQ}}^T + \frac{N_0}{2}\Sigma \right)^{-1} \mathbf{h}_{IQ,k_p} \, , \tag{4.7}$$

where $\mathbf{h}_{IQ,k_p}$ is the $(2k_p+p)$-th column of $\mathbf{H}_{IQ}$, i.e. the column corresponding to the decision delay k_p. The corresponding optimal MSE [17] is given by the $(2k_p+p)$-th diagonal element of $\frac{N_0}{2}\left(\frac{N_0}{2}\mathbf{I} + \mathbf{H}_{IQ}\Sigma^{-1}{\mathbf{H}_{IQ}}^T\right)^{-1}$.

4.2 Performance Analysis

In this section we present the theoretical performance analysis for our WL MMSE detector. The purpose is twofold. First, it is a tool for quick analysis of the effect of different system parameters on the expected performance, and second, it is used to verify our simulation implementation.

Instead of using the noise covariance matrix $\frac{N_0}{2}\Sigma$ in the calculation of the MMSE coefficients in Equation 4.7, we can get equivalent performance by first whitening the observation vector. This representation is easier to analyze, and can optionally be used as an alternative implementation variant for the actual detection. Using the Cholesky factorization

$$\Sigma = \mathbf{L}\mathbf{L}^T \,, \tag{4.8}$$

we get the equivalent system representation

$$\tilde{\mathbf{r}}_{IQ} = \mathbf{L}^{-1}\mathbf{r}_{IQ} = \mathbf{L}^{-1}\mathbf{H}_{IQ}\mathbf{b} + \mathbf{L}^{-1}\mathbf{n}_{IQ} = \tilde{\mathbf{H}}\mathbf{b} + \tilde{\mathbf{n}} \,. \tag{4.9}$$

The modified noise vector $\tilde{\mathbf{n}} = \mathbf{L}^{-1}\mathbf{n}_{IQ}$ has zero mean and covariance $\frac{N_0}{2}\mathbf{I}$, where $\mathbf{I}$ is the identity matrix. The decision variable d_p for user p is obtained using a filter $\tilde{\mathbf{w}}_p$, equivalent to the one presented in Equation 4.7:

$$\tilde{\mathbf{w}}_p = (\tilde{\mathbf{H}}\tilde{\mathbf{H}}^T + \frac{N_0}{2}\mathbf{I})^{-1}\tilde{\mathbf{h}}_{k_p} \tag{4.10}$$

$$d_p = \tilde{\mathbf{w}}_p^T\tilde{\mathbf{r}}_{IQ} = \tilde{\mathbf{w}}_p^T\tilde{\mathbf{H}}\mathbf{b} + \tilde{\mathbf{w}}_p^T\tilde{\mathbf{n}} = cb[k-k_p] + \mathbf{c}_I^T\mathbf{b}_I + \tilde{\mathbf{w}}_p^T\tilde{\mathbf{n}} \,, \tag{4.11}$$

where $b[k-k_p]$ is the desired symbol, $\mathbf{b}_I$ is the vector of interfering symbols from both tags, and c and $\mathbf{c}_I$ are the overall coefficients corresponding to them. By

approximating the total noise vector at the output of the equalizer

$$\mathbf{c}_I^T \mathbf{b}_I + \tilde{\mathbf{w}}_p^T \tilde{\mathbf{n}} \tag{4.12}$$

as a Gaussian vector, we can calculate the effective Signal to Noise Ratio (SNR) as

$$\eta = \frac{\mathbb{E}\{|cb[k-k_0]|^2\}}{\mathbb{E}\{|\mathbf{c_I}^T \mathbf{b_I} + \tilde{\mathbf{w}}^T \tilde{\mathbf{n}}|^2\}} = \frac{c^2}{\mathbf{c_I}^T \mathbf{c_I} + \frac{N_0}{2} \tilde{\mathbf{w}}^T \tilde{\mathbf{w}}} \,, \tag{4.13}$$

and the corresponding Bit Error Rate (BER)

$$\text{BER} = Q(\sqrt{\eta}) \,, \tag{4.14}$$

where $Q(\cdot)$ is the Gaussian Q function, This gives us a measure of the expected performance of the joint MMSE detector.

Figure 4.1 illustrates the effect of the timing offset τ and the phase offset θ on the expected joint MMSE performance (Equation 4.6), with no oversampling ($S = 1$) and $N = 9$, which means the WL filter has 18 coefficients. Both τ and θ provide us with means to distinguish between the signals in the complex plane. When $\tau = 0$ the pulse shapes of both signals are co-aligned, whereas $|\tau| = T$ means the derotation creates a phase difference of $\frac{\pi}{2}$ between the complex pulse shapes, i.e. they become orthogonal. This explains the observed symmetry around $\tau = 0$. Similarly when θ is a multiple of π the signals are phase-aligned, so it is reasonable to expect a symmetry around $\theta = \pi k$ as well. Alternatively we can observe similar trends in Figure 4.2, with oversampling but fewer symbols (i.e. $N = 4$, $S = 2$) keeping a similar number of coefficients in the WL filter.

Figure 4.3 illustrates the effect of the Signal to Interference Ratio (SIR) on

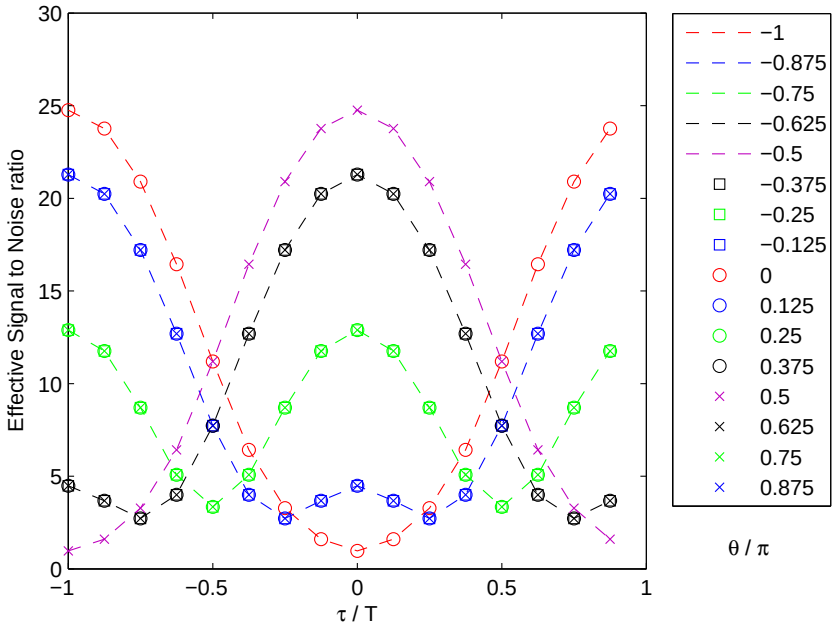

Figure 4.1: Expected performance of the joint MMSE detector, $N = 9$ and $S = 1$

the expected performance. We keep the power of the signal of interest constant, and change the relative power of the second tag. We observe the effective SNR at the output of the MMSE filter of the first tag. Since the filter is optimized for both interference and noise, we see better better performance when the interference is weaker.

In order to verify our simulation implementation, we compare the expected BER, as derived in Section 4.2, with the simulated BER results. We show the results for different channel parameters (τ, θ), and receiver parameters (N, S). In all simulations we assume the receiver has perfect channel state information available, and we use the same decision delay parameter k_p used in the analysis, determined

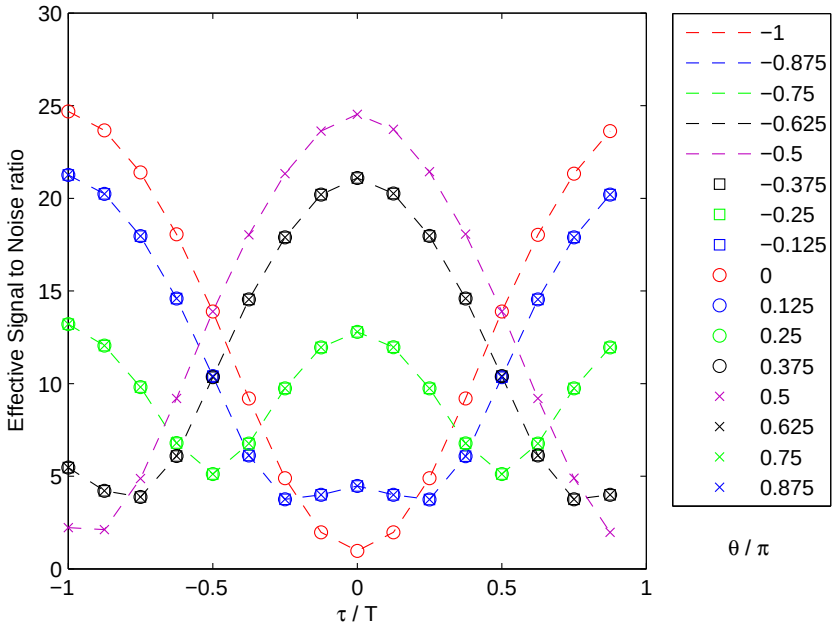

Figure 4.2: Expected performance of the joint MMSE detector, $N = 4$ and $S = 2$

by minimizing the MSE. Both the simulated and expected BER values for the first tag are plotted against $\frac{E_b}{N_0}$, where E_b is the received power per bit for the each tag, assuming the channel gain is 1. In these simulations we assumed θ includes all the phase contribution of the channel, and we gave both tags equal power.

Figure 4.4 shows the BER performance for both ($\tau = T/2$, $\theta = \pi$) and ($\tau = 0$, $\theta = -3\pi/8$). In both cases we see a good match between the calculated results and the simulated ones.

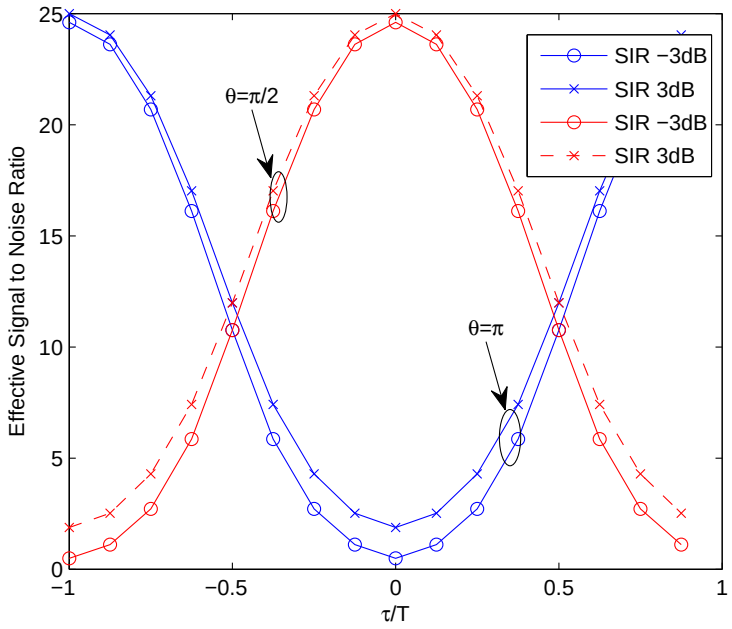

Figure 4.3: The effect of Signal to Interference Ratio (SIR) on the performance of the joint MMSE detector

4.3 Effect of Frequency Offset

We now study the effect of the frequency offset between the signals from the two tags as appears in Equation 3.15. The offset can be treated as a time-varying exponent that we incorporate into the channel matrix of Equation 4.1 as follows:

$$r[k] = \sum_{i=0}^{L} \begin{bmatrix} h_1[i] & e^{j2\pi\nu kT} h_2[i] \end{bmatrix} \begin{bmatrix} b_1[k-i] \\ b_2[k-i] \end{bmatrix} + n[k] \,. \tag{4.15}$$

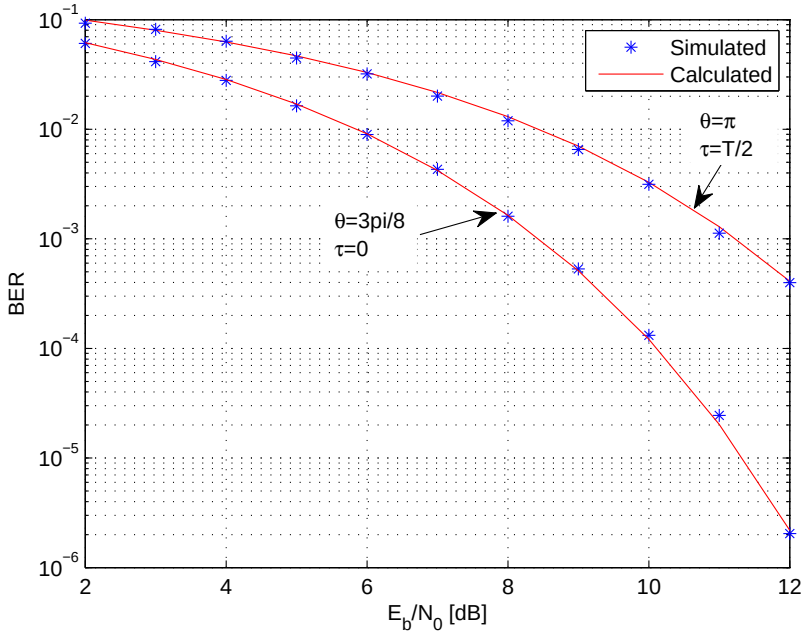

Figure 4.4: Joint MMSE Bit Error Rate (BER) results

The effect on receiver performance can be seen as averaging over different phase offsets θ. This time dependency propagates to $\mathbf{H}_{IQ}[i]$ of Equation 4.2, leading to

$$\mathbf{H}_{IQ,k}[i] = \begin{bmatrix} \Re\{h_1[i]\} & \Re\{e^{j2\pi\nu kT}h_2[i]\} \\ \Im\{h_1[i]\} & \Im\{e^{j2\pi\nu kT}h_2[i]\} \end{bmatrix}, \tag{4.16}$$

and to $\mathbf{H}_{IQ}$ of Equation 4.4

$$\mathbf{H}_{IQ} = \begin{bmatrix} \mathbf{H}_{IQ,k}[0] & \cdots & \mathbf{H}_{IQ,k}[L] & 0 & \cdots & 0 \\ 0 & \mathbf{H}_{IQ,k-1}[0] & \cdots & \mathbf{H}_{IQ,k-1}[L] & \cdots & 0 \\ \vdots & \ddots & \ddots & \ddots & \ddots & 0 \\ 0 & \cdots & 0 & \mathbf{H}_{IQ,k-N+1}[0] & \cdots & \mathbf{H}_{IQ,k-N+1}[L] \end{bmatrix}$$

The frequency-dependent expression for $\mathbf{H}_{IQ}$ should be used instead of the one in Equation 4.4 when calculating the MMSE coefficients using Equation 4.7. This means the MMSE coefficients change from symbol to symbol and need to be re-calculated during packet reception. However, since we are dealing with small frequency offsets ($\nu T \ll 1$), the effective channel changes slowly and the coefficients can be calculated for the first symbol and then updated using an adaptation technique (e.g. Least Mean Squares (LMS)), or calculated recursively using the method presented by Ahmed et al. [18]. Regardless of which adaptation method is used, the need to incorporate the frequency offset into the MMSE calculations means we must estimate it. Frequency offset estimation will be discussed in Chapter 7.

Chapter 5

Projection Filtering

This chapter presents an alternative MUD structure based on the Mono Interference Cancellation (MIC) algorithm proposed in [19]. We wish to analyze this method, and compare it to the joint MMSE detector we presented in the previous chapter. We use the same discrete-time signal model introduced in Chapter 3, and assume prefect channel knowledge. As with the previous receiver structure presented, we show the derivations for a symbol-spaced receiver, but note that it is straightforward to extend them to include oversampling.

5.1 Receiver Structure

The signal model used in Equation 4.1 is repeated here for reference. The symbol-spaced discrete-time received samples during the overlap between the packets are given by

$$r[k] = \sum_{i=0}^{L} b_1[k-i]h_1[i] + \sum_{i=0}^{L} b_2[k-i]h_2[i] + n[k] \,, \tag{5.1}$$

where $b_1[k]$ and $b_2[k]$ are the data symbols of the first and second tag respectively. In this scheme the primary user is first suppressed using a projection filter, whose output is then used to detect the secondary user. Initially we denote the first and second tags as primary and secondary respectively, but the roles can then be reversed in order to detect the data symbols of both tags.

We first pass the received samples through a projection filter with complex coefficients $p[k]$ and take the real part of the output, yielding

$$r_p[k] = \Re\{p[k] * r[k]\} \, . \tag{5.2}$$

Assuming $h_1[k]$ is known, and defining $h_{1_I}[k]$ and $h_{1_Q}[k]$ as the real and imaginary parts of $h_1[k]$ respectively, we perform zero forcing with respect to the primary user by choosing

$$p[k] = -jq[k] * (h_{1_I}[k] - jh_{1_Q}[k]) = q[k] * (-h_{1_Q}[k] - jh_{1_I}[k]) \, , \tag{5.3}$$

where $q[k]$ is an arbitrary real-valued filter. The selected coefficients of $q[k]$ do not affect its zero forcing capabilities, and can therefore be used to add noise suppression for the secondary user. In our simulations we simply used $q[k] = \delta[k]$.

The projected signal can be written as

$$r_p[k] = p_I[k] * r_I[k] - p_Q[k] * r_Q[k] = \sum_i b_2[k-i]h_p[i] + n_p[k] \, , \tag{5.4}$$

where $p_I[k]$ and $p_Q[k]$ are the real and imaginary parts of $p[k]$ respectively, $n_p[k] = p_I[k] * n_I[k] - p_Q[k] * n_Q[k]$ are the projected noise samples (the subscripts I and Q represent real and imaginary parts), and the overall impulse response for the

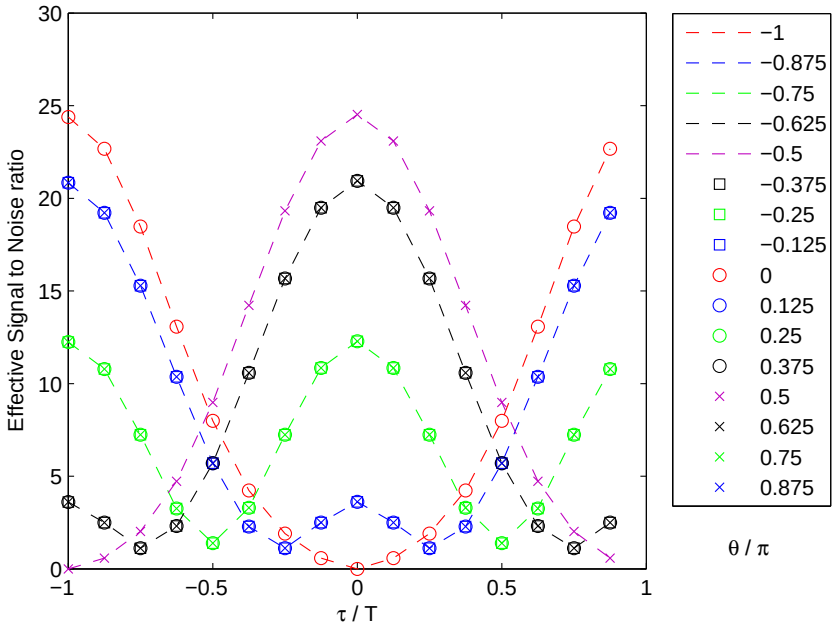

Figure 5.1: Expected performance for projection filtering, $N = 9$ and $S = 1$.

secondary user is given by

$$h_p[k] = p_I[k] * h_{2_I}[k] - p_Q[k] * h_{2_Q}[k] \; . \tag{5.5}$$

Note that $n_p[k]$ is a coloured noise, with covariance $\frac{N_0}{2}\Sigma_p$. Based on the representation in Equation 5.4, we can now estimate the transmitted sequence $b_2[k]$ using an MMSE linear equalizer. The filter coefficients can be calculated as in Equation 4.7, using $h_p[k]$ instead of $h[k]$.

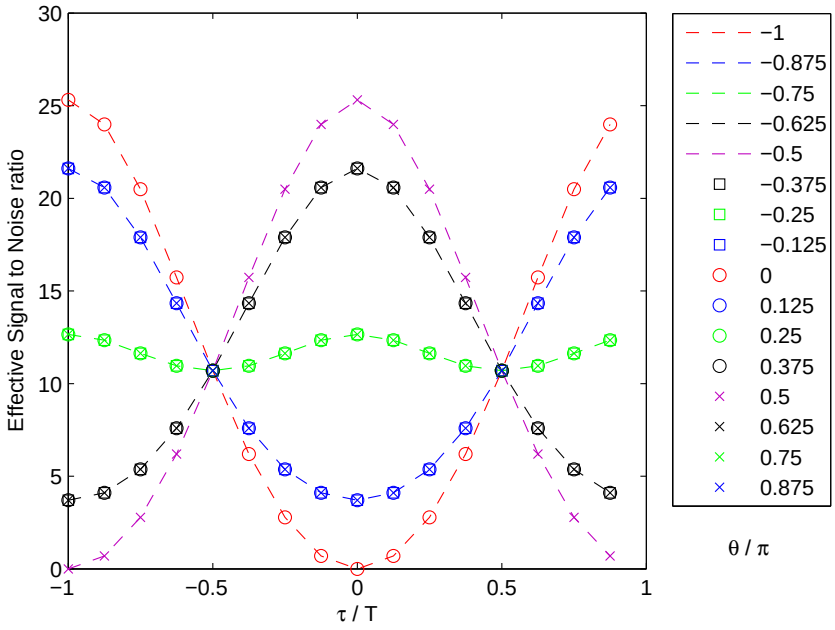

Figure 5.2: The MFB performance measure, $S = 1$.

5.2 Performance Analysis

In this section we use two performance measures to evaluate the projection filtering approach. The first is the expected MMSE performance, which is derived in the same way as in Section 4.2. The second measure is the Matched Filter Bound (MFB), which gives an upper bound on the performance by assuming only one symbol is transmitted through the system (thus eliminating the effect of Inter Symbol Interference (ISI)). We include this additional measure here since the overall impulse response $h_p[k]$ has a longer support, and is therefore more sensitive to ISI. We wish to observe the effect of opting to use a finite linear equalizer instead of a Viterbi equalizer. In order to evaluate the MFB we need to observe a vector of

received samples

$$\mathbf{r}_p = \mathbf{h}_p b + \mathbf{n}_p \ , \tag{5.6}$$

where $\mathbf{h}_p$ contains the non-zero elements of the overall impulse response $h_p[k]$. $\mathbf{n}_p$ is a vector of Gaussian noise samples with zero mean and covariance $\frac{N_0}{2}\Sigma_p$. Using the Cholesky factorization

$$\Sigma_p = \mathbf{L}\mathbf{L}^T \ , \tag{5.7}$$

we consider the whitened observation vector

$$\tilde{\mathbf{r}}_p = \mathbf{L}^{-1}\mathbf{r}_p = \mathbf{L}^{-1}\mathbf{h}_p b + \mathbf{L}^{-1}\mathbf{n}_p = \tilde{\mathbf{h}}_p b + \tilde{\mathbf{n}}_p \ . \tag{5.8}$$

The modified noise vector $\tilde{\mathbf{n}}_p$ has zero mean and covariance $\frac{N_0}{2}\mathbf{I}$. The effective SNR of the MFB is given by

$$\eta_{MFB} = \frac{2\left\|\tilde{\mathbf{h}}_p\right\|^2}{N_0} \ , \tag{5.9}$$

and the corresponding BER is

$$\mathrm{BER}_{MFB} = Q(\sqrt{\eta_{MFB}}) \ . \tag{5.10}$$

Figure 5.1 shows the effect of the timing offset τ and the phase offset θ on the expected performance. As foreseen we observe a symmetry around $\tau = 0$, when the pulse shapes are aligned and the only way to distinguish between the signals is through the phase θ. As mentioned in Section 4.2, when $|\tau| = T$ the derotation creates a phase difference of $\frac{\pi}{2}$ between the complex pulse shapes and they become orthogonal. This orthogonality, as well as the one obtained by the phase offset itself $\theta = \pm\pi$, yields the best performance. In cases of orthogonality we achieve the best

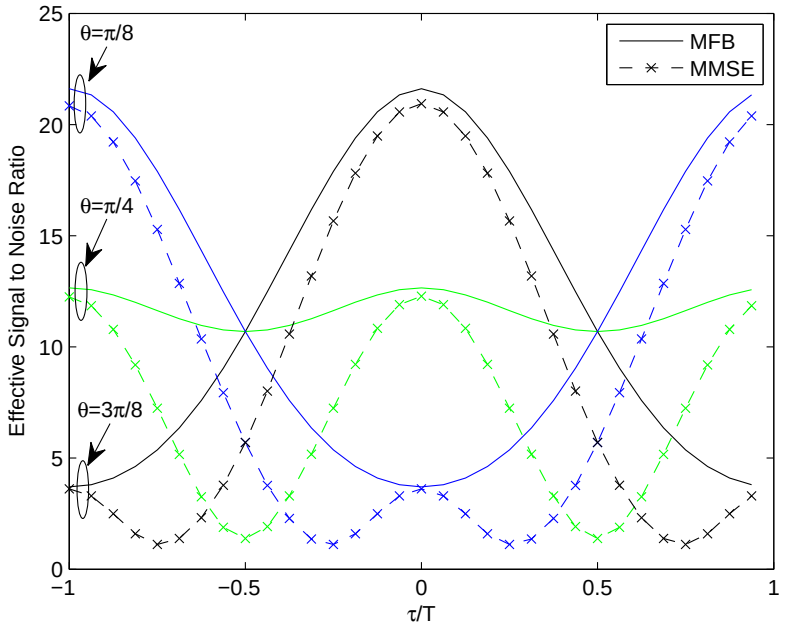

Figure 5.3: Comparison between MMSE and MFB performance measures

match with the results of the previous chapter, since we do not suffer from zero-forcing-induced noise enhancement. The most significant effect of the zero forcing projection filter is observed when the pulse shapes are aligned - it suppresses both signals and we get an effective signal to noise ratio of 0. We can see that the results in Section 4.2 are at least as good and in many cases better than the projection filtering results, since the interference and noise suppression are jointly optimized for minimum MSE.

Figure 5.2 illustrates the effect of τ and θ on the MFB performance measure. We observe the same symmetries as before. Figure 5.3 compares the MMSE and MFB performance metrics for selected channel parameters. When the pulse shapes themselves are aligned ($\tau = 0, \pm T$), the signals can only be distinguished by a

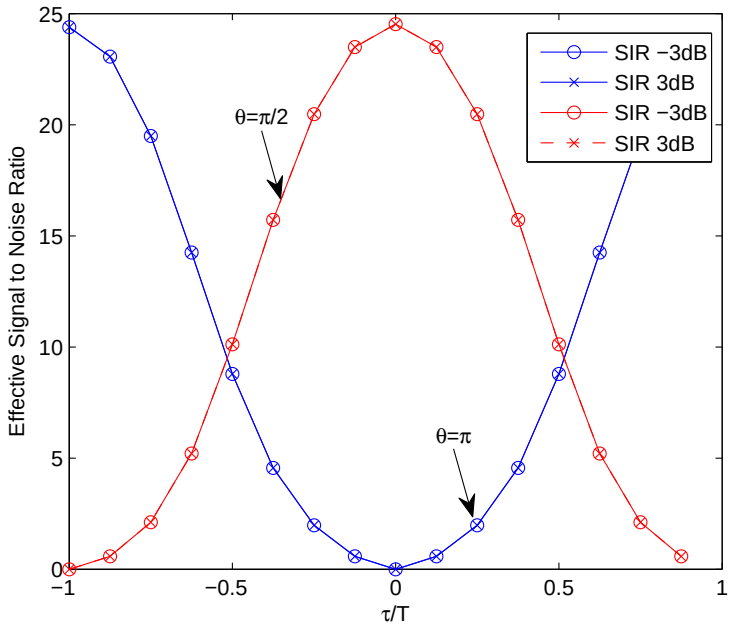

Figure 5.4: Effect of Signal to Interference Ratio (SIR) on the performance of the projection filtering detector.

phase offset (no ISI) and the difference between the MFB and MMSE performance is minimal. In other cases we suffer from ISI and the difference between the perfromance measures is more significant.

Figure 5.4 illustrates the effect of the SIR on the expected performance. We keep the power of the signal of interest constant, and change the relative power of the second tag. We observe the effective SNR at the output of the MMSE filter of the first tag. Since the projection filter suppresses the interference, the performance does not depend on the interference level. In cases where the interference power is low we actually suffer from performance degradation. Since we are ultimately interested in detecting both packets, the joint MMSE scheme seems more suitable

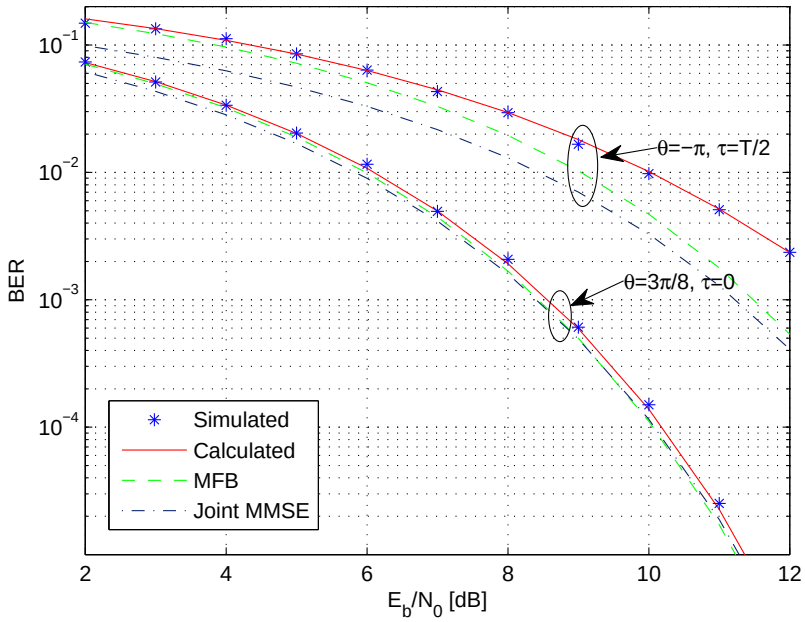

Figure 5.5: Projection filtering Bit Error Rate (BER) performance

to our needs.

In order to verify our simulation implementation, we compare the expected BER with respect to the Gaussian noise level N_0, as derived in Section 5.2, with our simulated BER results. Figure 5.5 shows the BER performance for $\tau = T/2$ and $\theta = -\pi$, as well as for $\tau = 0$ and $\theta = 3\pi/8$. The MFB results and the expected BER of the joint MMSE detector are given for comparison. We see a good fit between our calculated and simulated BER values. Once again we observe a more significant gap between the projection filtering results and the MFB when the pulse shapes are not aligned ($\tau = T/2$). The benefits of using the joint MMSE detector are demonstrated here as well, since its results clearly exceeds those of the projection filtering scheme.

Chapter 6

Channel Estimation

In the previous chapters we assumed that channel coefficients are perfectly known. This chapter discusses the method we use for estimating these coefficients. We start by assuming the second packet is received after the header of the first packet has been received, as depicted in Figure 6.1. In this case we are synchronized with the first tag and have an estimate of its channel coefficients. We now wish to estimate the channel coefficients of the second tag using its header. In Section 6.4 we will discuss the channel estimation of the first tag, and will also explain what modifications are needed when the headers overlap. At this stage we assume the receiver knows at which symbol duration the interference starts. The acquisition process will be discussed in Chapter 7.

6.1 System Model

Let us look at the received signal as defined in Equation 4.1:

$$r[k] = \sum_{i=0}^{L} b_1[k-i]h_1[i] + \sum_{i=0}^{L} b_2[k-i]h_2[i] + n[k] \; . \tag{6.1}$$

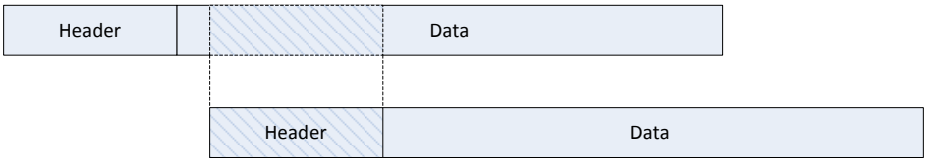

Figure 6.1: Structure and relative positions of the received packets. Channel estimation is performed during reception of the striped region

In other multiuser systems (e.g. cellular networks or even passive RFID systems) the different users transmit their training sequences simultaneously, and those can be used to perform joint channel estimation. In our case we assume the first tag's header has already been received, its overall channel coefficients $h_1[k]$ are known, and we are now receiving its unknown data symbols $b_1[k]$. On the other hand, we are now in the process of receiving the second tag's known header $b_2[k]$ and want to estimate its coefficients $h_2[k]$.

We look at a window of $K-L+1$ received samples that are affected by the $K+1$ header symbols, and rewrite Equation 6.1 in matrix form as

$$\mathbf{r} = \mathbf{H}_1\mathbf{b}_1 + \mathbf{B}_2\mathbf{h}_2 + \mathbf{n}\,, \tag{6.2}$$

where

$$\begin{aligned}
\mathbf{r} &= \begin{bmatrix} r[K] & \cdots & r[L] \end{bmatrix}^T \\
\mathbf{n} &= \begin{bmatrix} n[K] & \cdots & n[L] \end{bmatrix}^T \\
\mathbf{h}_2 &= \begin{bmatrix} h[0] & \cdots & h[L] \end{bmatrix}^T \\
\mathbf{b}_1 &= \begin{bmatrix} b_1[K] & \cdots & b_1[K-L] \end{bmatrix}^T ,
\end{aligned} \tag{6.3}$$

the symbol matrix $\mathbf{B}_2$ includes the $K+1$ known header symbols

$$\mathbf{B}_2 = \begin{bmatrix} b_2[K] & b_2[K-1] & \cdots & b_2[K-L] \\ \vdots & & \ddots & \vdots \\ b_2[L+1] & b_2[L] & \cdots & b_2[1] \\ b_2[L] & b_2[L-1] & \cdots & b_2[0] \end{bmatrix} , \tag{6.4}$$

and the channel matrix $\mathbf{H}_1$ is constructed from the known (or estimated) channel coefficients $h_1[k]$

$$\mathbf{H}_1 = \begin{bmatrix} h_1[0] & \cdots & h_1[L] & 0 & \cdots & 0 \\ 0 & h_1[0] & \cdots & h_1[L] & \cdots & 0 \\ \vdots & \ddots & \ddots & \ddots & \ddots & 0 \\ 0 & \cdots & 0 & h_1[0] & \cdots & h_1[L] \end{bmatrix} . \tag{6.5}$$

We construct the combined linear system representation

$$\mathbf{r} = \begin{bmatrix} \mathbf{H}_1 & \mathbf{B}_2 \end{bmatrix} \begin{bmatrix} \mathbf{b}_1 \\ \mathbf{h}_2 \end{bmatrix} + \mathbf{n} = \mathbf{A}\mathbf{x} + \mathbf{n} \,. \tag{6.6}$$

Since the noise vector $\mathbf{n}$ is coloured, we create a whitened observation vector

$$\tilde{\mathbf{r}} = \mathbf{L}^{-1}\mathbf{r} = \mathbf{L}^{-1}\mathbf{A}\mathbf{x} + \mathbf{L}^{-1}\mathbf{n} = \tilde{\mathbf{A}}\mathbf{x} + \tilde{\mathbf{n}} \,, \tag{6.7}$$

where $\tilde{\mathbf{A}} = \mathbf{L}^{-1}\mathbf{A}$, $\tilde{\mathbf{H}}_1 = \mathbf{L}^{-1}\mathbf{H}_1$, and $\tilde{\mathbf{B}}_2 = \mathbf{L}^{-1}\mathbf{B}_2$.

6.2 Initial Estimation

One of the common methods for channel estimation given a training sequence is Least Squares (LS) estimation [20]. The LS estimate of our parameter vector $\mathbf{x}$ is given by

$$\hat{\mathbf{x}}_{LS} = \underset{\mathbf{x}}{\operatorname{argmin}} \left\| \tilde{\mathbf{r}} - \tilde{\mathbf{A}}\mathbf{x} \right\|^2 = \tilde{\mathbf{A}}^{\dagger}\tilde{\mathbf{r}} \,, \tag{6.8}$$

where $\mathbf{A}^{\dagger}$ is the pseudo-inverse of $\mathbf{A}$. This estimator does not take advantage of the fact that the elements of $\mathbf{x}$ that correspond to the data symbols are real-valued. We can therefore improve the estimate by employing WL processing as we did in Section 4.1. Each complex entry in Equation 6.7 is decomposed into its real and imaginary components and the matrix representation can be rewritten as:

$$\mathbf{r}_{IQ} = \mathbf{H}_{1_{IQ}}\mathbf{b}_1 + \mathbf{B}_{2_{IQ}}\mathbf{h}_{2_{IQ}} + \mathbf{n}_{IQ} \tag{6.9}$$

$$= \begin{bmatrix} \mathbf{H}_{1_{IQ}} & \mathbf{B}_{2_{IQ}} \end{bmatrix} \begin{bmatrix} \mathbf{b}_1 \\ \mathbf{h}_{2_{IQ}} \end{bmatrix} + \mathbf{n} = \mathbf{A}_{IQ}\mathbf{x}_{IQ} + \mathbf{n}_{IQ} \,, \tag{6.10}$$

where $\mathbf{r}_{IQ}$, $\mathbf{n}_{IQ}$, $\mathbf{H}_{1_{IQ}}$ and $\mathbf{h}_{2_{IQ}}$ are constructed by taking each complex element e in the vectors $\tilde{\mathbf{r}}$, $\tilde{\mathbf{n}}$, the matrix $\tilde{\mathbf{H}}_1$, and the vector $\mathbf{h}_2$ respectively and expanding it to its real and imaginary components

$$\begin{bmatrix} \Re\{e\} & \Im\{e\} \end{bmatrix}^T , \tag{6.11}$$

and $\mathbf{B}_{2_{IQ}}$ is constructed by taking each complex element b in $\tilde{\mathbf{B}}_2$ and expanding it to

$$\begin{bmatrix} \Re\{b\} & -\Im\{b\} \\ \Im\{b\} & \Re\{b\} \end{bmatrix} . \tag{6.12}$$

The LS estimate of the real parameter vector $\mathbf{x}_{IQ}$ is given by

$$\hat{\mathbf{x}}_{IQ} = \begin{bmatrix} \hat{\mathbf{b}}_1 \\ \hat{\mathbf{h}}_{2_{IQ}} \end{bmatrix} = \mathbf{A}_{IQ}{}^{\dagger}\mathbf{r}_{IQ} . \tag{6.13}$$

In order to improve the channel estimate, we use the fact that the elements of $\mathbf{b}_1$ can only take the values ± 1, and therefore slice the elements of $\hat{\mathbf{b}}_1$ to the nearest symbols. If any of the symbols are known due to an overlap between the headers (in this case some of the symbols in $\mathbf{b}_1$ are part of the header and some are unknown data symbols), we can use the known values instead of the sliced value. We now generate a vector of residual observations

$$\mathbf{r}_{IQ,res} = \mathbf{r}_{IQ} - \mathbf{H}_{1_{IQ}}\hat{\mathbf{b}}_{1,sliced} = \mathbf{B}_{2_{IQ}}\mathbf{h}_{2_{IQ}} + \mathbf{n}_{IQ,res} \tag{6.14}$$

that can be used to generate a better estimate of $\mathbf{h}_2$.

6.3 Improved Estimation

After subtracting the contribution of the first tag, we can improve the channel estimation by exploiting our knowledge of the channel structure as well as our flat-fading assumption. From Equation 6.14 we have

$$\tilde{\mathbf{r}}_{res} = \tilde{\mathbf{B}}_2 \mathbf{h}_2 + \tilde{\mathbf{n}}_{res} \,, \tag{6.15}$$

so the LS estimate of $\mathbf{h}_2$ is given by $\left(\tilde{\mathbf{B}}_2\right)^{\dagger} \tilde{\mathbf{r}}_{res}$. As can be seen in Equation 3.14, the overall channel coefficients depend on the pulse shape autocorrelation function and an unknown complex channel gain:

$$h[k] = \alpha e^{j\theta} j^{-k} R_{ff}\left(kT - \tau_m\right) \,. \tag{6.16}$$

Due to this derotation structure we know that the phase of each channel coefficient is linear with its time index, i.e. the phase difference between the coefficients is constant. We can therefore express the channel coefficients as

$$\mathbf{h}_2 = \mathbf{P} \rho e^{j\phi} \,, \tag{6.17}$$

where ρ is a real-valued vector, ϕ is a common phase, and $\mathbf{P}$ is a diagonal matrix that includes the contribution of the derotation $\mathbf{P} = \text{diag}(j^{-[0,..,L]})$. Equation 6.15 becomes a complex least squares problem with a constrained phase, so we can use the method presented in [21] to solve it. From the new problem formulation

$$\mathbf{r}_{res} = \left(\mathbf{B}_2 \mathbf{P}\right) \rho e^{j\phi} + \mathbf{n}_{res} \,, \tag{6.18}$$

we obtain an estimate of the complex phase and the real coefficients

$$\hat{\phi} = \frac{1}{2}\angle\left\{\left(\left(\mathbf{B}_2\mathbf{P}\right)^H \mathbf{r}_{res}\right)^T \mathbf{M}^{-1}\left(\mathbf{B}_2\mathbf{P}\right)^H \mathbf{r}_{res}\right\} \tag{6.19}$$

$$\hat{\rho} = \mathbf{M}^{-1}\Re\left\{\left(\mathbf{B}_2\mathbf{P}\right)^H \mathbf{r}_{res} e^{-j\hat{\phi}}\right\}$$

with $\mathbf{M}$ defined as

$$\mathbf{M} = \Re\left\{\left(\mathbf{B}_2\mathbf{P}\right)^H \left(\mathbf{B}_2\mathbf{P}\right)\right\} \tag{6.20}$$

To account for frequency offsets between the two tags, we simply update Equation 6.1 as follows:

$$r[k] = \sum_{i=0}^{L} b_1[k-i]h_1[i] + \sum_{i=0}^{L} e^{j2\pi\nu kT} b_2[k-i]h_2[i] + n[k]\ . \tag{6.21}$$

and then Equation 6.2 becomes

$$\mathbf{r} = \mathbf{H}_1\mathbf{b}_1 + \mathbf{C}_\nu\mathbf{B}_2\mathbf{h}_2 + \mathbf{n}\ , \tag{6.22}$$

where $\mathbf{C}_\nu$ contains the frequency correction terms on its diagonal

$$\mathbf{C}_\nu = \mathrm{diag}\left\{e^{j2\pi\nu[0\ldots K]T}\right\} \tag{6.23}$$

By using our frequency offset estimation and replacing $\mathbf{B}_2$ with $\mathbf{C}_\nu\mathbf{B}_2$, the rest of our derivations remain valid.

Finally, we combine the improvements described above in the following iterative estimation scheme:

1. Generate initial estimates of the channel coefficients $\hat{\mathbf{h}}_2$ and the data symbols

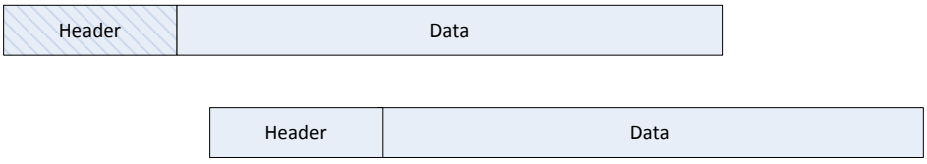

(a) serial

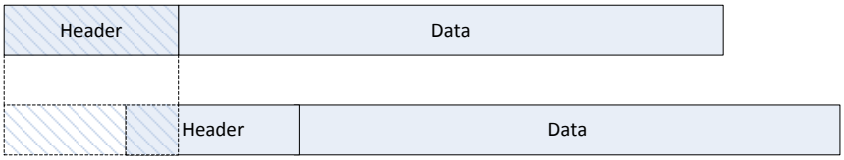

(b) overlapping

Figure 6.2: Structure and relative positions of the received packets. Channel estimation for the first packet is performed during reception of the striped region

$\hat{\mathbf{b}}_1$ according to Equation 6.13.

2. Slice the data symbols to the nearest BPSK symbol, and update the vector of residual observation as in Equation 6.14.

3. Estimate the channel coefficients using the constrained phase solution in Equation 6.19.

4. Update the data symbols estimation $\hat{\mathbf{b}}_1 = \mathbf{H}_1^{\dagger}\left(\mathbf{r} - \mathbf{B}_2\hat{\mathbf{h}}_2\right)$

5. If the sliced value of any of the symbols changed, repeat the process from step 2.

6.4 Channel Estimation in the Single User Case

Before detecting a collision, we assume only one packet is received and have to detect its channel coefficients. If the header of the first tag is received before the interference starts, as illustrated in Figure 6.2a, the observation vector can be expressed as

$$\mathbf{r} = \mathbf{B}_1 \mathbf{h}_1 + \mathbf{n} \,, \tag{6.24}$$

where now the symbol matrix $\mathbf{B}_1$ includes the known header symbols

$$\mathbf{B}_1 = \begin{bmatrix} b_1[K] & b_1[K-1] & \cdots & b_1[K-L] \\ \vdots & & \ddots & \vdots \\ b_1[L+1] & b_1[L] & \cdots & b_1[1] \\ b_1[L] & b_1[L-1] & \cdots & b_1[0] \end{bmatrix} . \tag{6.25}$$

The improvements described Section 6.3 over LS estimation can be used for single user channel estimation as well. We therefore use the constrained phase solution to estimate the channel of the first tag before detecting a collision. Since in this case we do not have the contribution of interfering data symbols from another tag, we do not need to use the iterative scheme.

In case of an overlap between the headers, we have partial interference from the second tag. If we detect the start of a second packet at a relative delay of k_d symbols, the signal model in Equation 6.24 can be enhanced by incorporating the interference model. We do this by creating a second symbol matrix $\mathbf{B}_2$ of the same structure as before, only now the elements $b_2[k]$ include zeros for $k < k_d$, and

header symbols for $k_d \leq k \leq K$. We construct the combined linear system

$$\mathbf{r} = \begin{bmatrix} \mathbf{B}_1 & \mathbf{B}_2 \end{bmatrix} \begin{bmatrix} \mathbf{h}_1 \\ \mathbf{h}_2 \end{bmatrix} + \mathbf{n} = \mathbf{B}\mathbf{h} + \mathbf{n} \,. \tag{6.26}$$

The LS estimate of the combined channel vector $\mathbf{h}$ is given by

$$\hat{\mathbf{h}} = \begin{bmatrix} \hat{\mathbf{h}}_1 \\ \hat{\mathbf{h}}_2 \end{bmatrix} = \mathbf{B}^{\dagger}\mathbf{r} \,. \tag{6.27}$$

We extract the estimate of the first channel $\hat{\mathbf{h}}_1$ and use it for the rest of the detection process. The final estimation of $\mathbf{h}_2$ is performed using the iterative scheme of Section 6.3.

6.5 Channel Estimation Performance

In order to demonstrate the effect of the channel estimation scheme described in Section 6.3 on the performance, we evaluate the effective SNR at the output of the Joint MMSE receiver, as described in Section 4.2. We compare the effective SNR when using the known channel coefficients to calculate the MMSE filter against the effective SNR when using the estimated coefficients. The resulting SNR values are averaged over $10,000$ simulations with different noise realizations. Figure 6.3 shows the difference in dB (the effective SNR loss) vs. the background noise level for example channel realizations ($\tau = \frac{3T}{4}$, $\theta = -\frac{\pi}{4}$, $\alpha = 1$; $\tau = 0$, $\theta = \frac{3\pi}{8}$, $\alpha = 1$). We show the improvement the different stages offer, from the initial estimate, through slicing the data symbols $\hat{\mathbf{b}}_1$, to using the constrained phase solution. As expected we see higher degradation when $\mathrm{E_b}/N_0$ is low, due to the poor initial

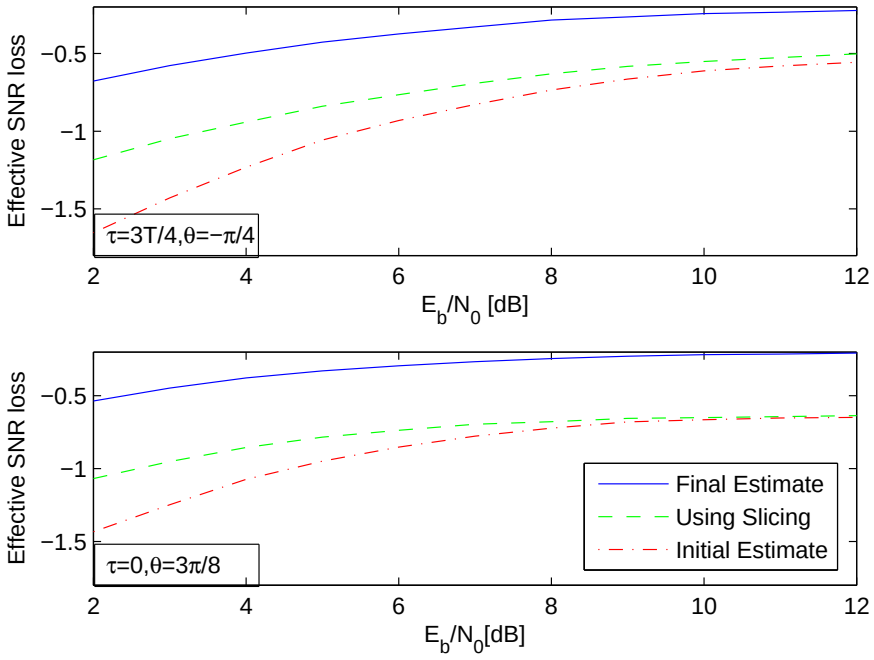

Figure 6.3: Average SNR loss at the output of the MMSE receiver due to channel estimation errors

estimation.

Chapter 7

Packet Acquisition

In the previous chapters we assumed that we know in which symbol interval the collision starts (the relative delay in symbol periods k_d), as seen in Figure 7.1. We also assumed that we know the relative frequency offset between the packets. In this chapter we describe how to estimate the delay k_d and the frequency offset ν using the known header symbols.

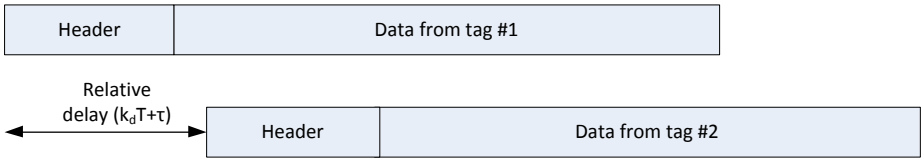

Figure 7.1: The known header is used to detect the beginning of a new packet and estimate the relative delay k_d

7.1 Header Detection

In order to determine the symbol in which a new packet starts we use the discrete-time derotated symbols $r[k]$. One of the common ways to perform frame synchronization is to consider the correlation of the received samples with the known header sequence $b[k]$ [22]

$$R[k] = \sum_{i=0}^{K} r[k+i]b[i] \, . \tag{7.1}$$

The absolute value of the correlator output peaks at the frame start. In order to better support frequency offsets, the D-lag differential version

$$R_D[k] = \sum_{i=0}^{K-D} r[k+i]r^*[k+i+D]b[i]b[i+D] \, . \tag{7.2}$$

can be used instead. We use the decision variable proposed by Corazza and Pedone [23], which can be written as

$$d[k] = R_0[k] + 2\sum_{D=1}^{D_{max}} |R_D[k]| \, , \tag{7.3}$$

where D_{max} is a design parameter, and compare it to a threshold value. Once the detection metric crosses the threshold, we search for its maximum point within a certain time-window. The time index of that maximum is used as the estimated symbol delay.

When the first packet is acquired, we start demodulating it using a single user detector. The detected bits and the first user's channel coefficients $h_1[k]$ are used to

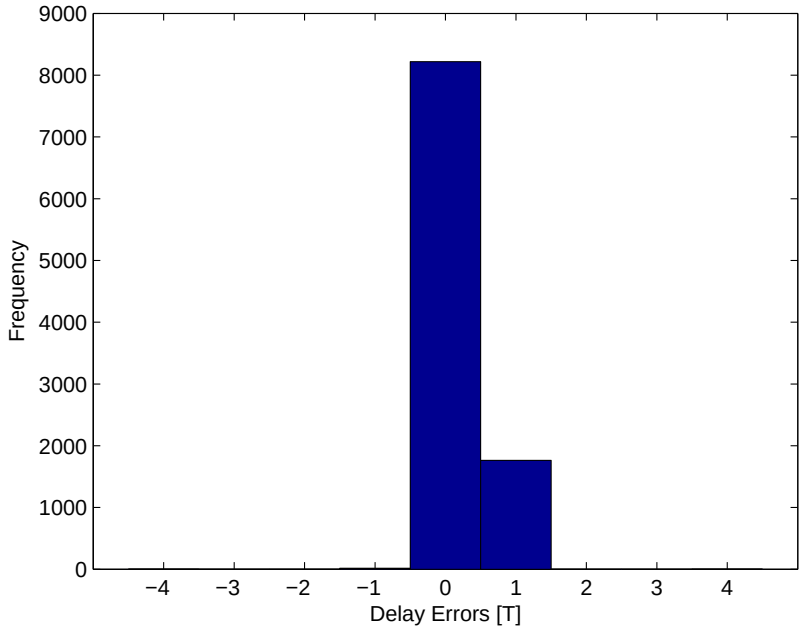

Figure 7.2: Histogram of delay estimation errors, E_b/N_0=12dB and SIR=0dB

generate the residual samples

$$r_{res}[k] = r[k] - \sum_{i=0}^{L} \hat{b}_1[k-i]h_1[i] = \sum_{i=0}^{L} b_2[k-i]h_2[i] + z[k] \,, \tag{7.4}$$

where $\hat{b}_1[k]$ contains the known header bits for $k < K$ and the detected bits afterwards. We then use the correlation metric in Equation 7.3 to search for another instance of the header. If there is an overlap between the headers, the residual samples around the delay index k_d are based on the actual header symbols and not on decisions.

We evaluated the performance of this header detection scheme by running simulations for $10,000$ iterations, where the channel phase θ, as well as the relative

delay between the packets $k_dT + \tau$ were randomized. The channel gain α was fixed according to the desired SIR, and tested for SIR levels of 0dB and $\pm$6dB. Figure 7.2 shows the results of delay estimation for the second user when the SIR level is set to 0dB. Note that delay errors $-1 \leq \Delta k_d \leq 1$ should not affect the overall performance, since channel estimation can compensate for them. Table 7.1 lists the probability of erroneous delay estimation ($|\Delta k_d| > 1$) for different SIR levels. We encounter more errors when the second tag is stronger due to the inherent asymmetry of our solution. We will assess the effect of delay estimation on overall system performance in Chapter 8.

E_b/N_0[dB]	SIR[dB]	Probability of error
12	0	5×10^{-4}
30	0	0
30	6	0
30	-6	3×10^{-2}

Table 7.1: Probability of error in delay estimation

7.2 Frequency Estimation

The packet preamble suggested by the standard is composed of 32 alternating symbols of -1 and 1. We can use this repetitive structure to estimate the frequency offset. Consider the D-lag differential samples affected by the preamble symbols

$$\begin{aligned} r[k]r^*[k+D] &\approx e^{j2\pi\nu TD} \sum_{i=0}^{L} b[k-i]h[i] \sum_{l=0}^{L} b[k+D-l]h[i] \\ &= e^{j2\pi\nu D}(-1)^D \left| \sum_{i=0}^{L} b[k-i]h[i] \right|^2 \end{aligned} \tag{7.5}$$

We can use the angles

$$\Omega_D \approx \angle(-1)^D r[k] r^*[k+D] = 2\pi\nu TD \tag{7.6}$$

to obtain an estimate of the frequency offset, according to the Fitz [24] estimator

$$\hat{\nu} = \frac{1}{2\pi T} \frac{6}{D_{max}(D_{max}+1)(2D_{max}+1)} \sum_{D=1}^{D_{max}} D\Omega_D \tag{7.7}$$

The performance of the frequency estimator was evaluated by running $10,000$ simulations, with randomized values for the channel phase θ and for the relative delay between packets where the channel phase θ and the relative delay between the packets were randomized. The channel gain was fixed to $\alpha = 1$. Figure 7.3 shows the results for $E_b/N_0 = 12$dB.

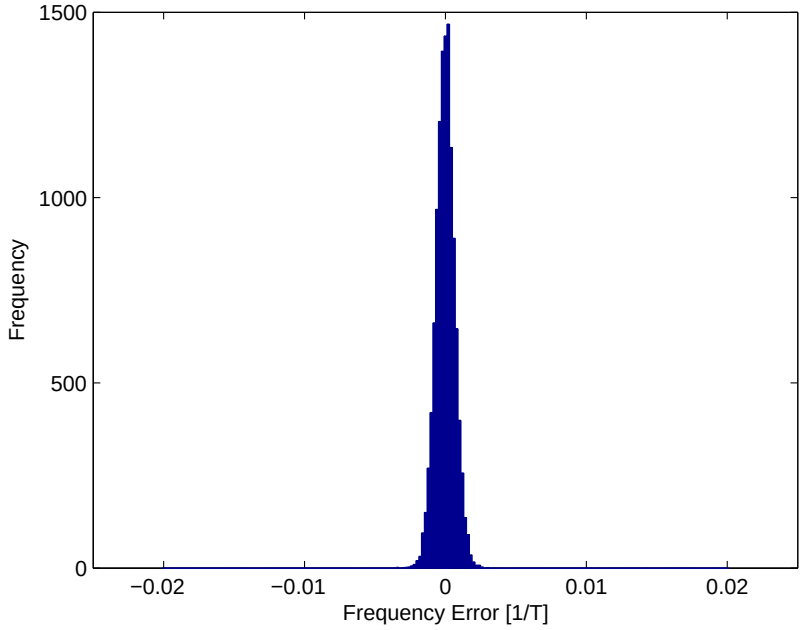

Figure 7.3: Histogram of frequency offset estimation errors, $E_b/N_0 = 12$dB

Chapter 8

Full System Simulation

In this chapter we construct the full multiuser system, which combines the components described in the previous chapters. We then present simulation results comparing the Packet Error Rate (PER) of a Single User Detection (SUD) system with that of our proposed MUD system.

8.1 System Overview

Figure 8.1 presents a flowchart of the entire proposed system, using the building blocks described in previous chapters. We start with single user packet acquisition. Once the first packet is acquired, we run single user channel estimation and begin demodulating the data symbols of the first tag. These are fed back into the packet acquisition block, which looks for another packet as described in Chapter 7. If we detect the presence of a second packet, we check the estimated symbol delay between the packets. If there is an overlap between the headers, as depicted in Figure 6.2b, we repeat the channel estimation process for the first tag using the method from Section 6.4. We then proceed to estimate the channel of the second tag using

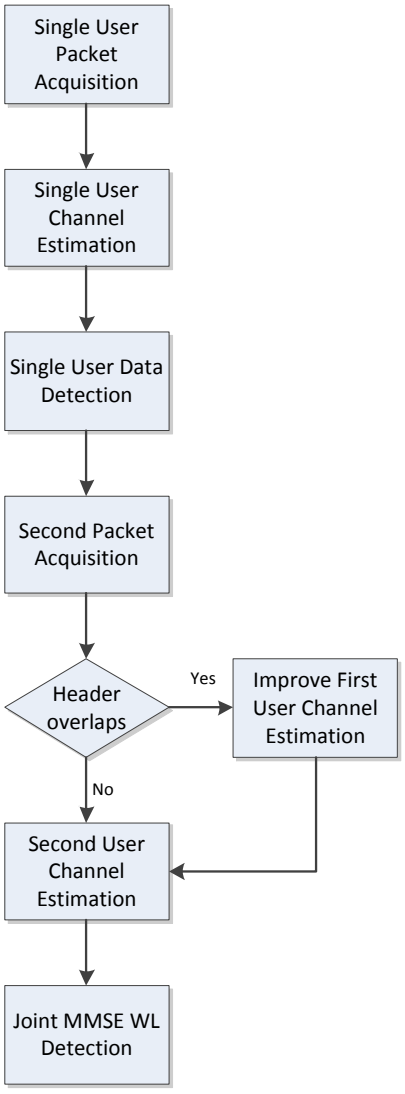

Figure 8.1: Flowchart of the full MUD system

the iterative method described in Section 6.3. The estimated parameters are then used to jointly detect the data symbols of both tags according to Chapter 4.

8.2 Simulation Results

We ran performance simulation on the integrated system in several scenarios. First, we tested the performance without any background noise. In each iteration of the simulation we randomized the relative delay between the two packets ($k_d T + \tau$) according to an exponential distribution with a parameter λ, as defined in Equation 2.3. While these simulations do not capture collisions involving more than two packets, they give us good insight about the system's ability to jointly detect two packets. We also randomized the complex channel phase (θ) uniformly, and set the channel gain (α) according to the desired SIR. Table 8.1 contains PER results for both a SUD solution and our suggested MUD scheme in different load settings. Looking at the results, there are several observations we can make. First, con-

λ	SIR [dB]	Collision Rate	SUD PER			MUD PER		
			User 1	User 2	Total	User 1	User 2	Total
0.2	0	0.1871	0.1372	0.1871	0.1621	0.0004	0.0006	0.0005
	6		0.0000	0.1871	0.0936	0.0000	0.0579	0.0290
	-6		0.1847	0.1871	0.1859	0.0945	0.0244	0.0595
0.5	0	0.3968	0.3081	0.3968	0.3525	0.0020	0.0022	0.0021
	6		0.0000	0.3968	0.1984	0.0000	0.1290	0.0645
	-6		0.3917	0.3968	0.3942	0.1990	0.0595	0.1292
1	0	0.6372	0.5204	0.6372	0.5788	0.0037	0.0047	0.0042
	6		0.0000	0.6372	0.3186	0.0000	0.2214	0.1107
	-6		0.6296	0.6372	0.6334	0.3195	0.0989	0.2092

Table 8.1: Noise-free Packet Error Rate (PER)

trary to our assumptions in Section 2.1, some of the colliding packets are detected properly by the SUD system and likewise our MUD solution is not error free. This happens because our original analysis was only based on MAC-layer reasoning, and disregarded signal characteristics. As previously discussed in Chapter 4 the MUD capabilities depend on how difficult it is to distinguish between the two signals,

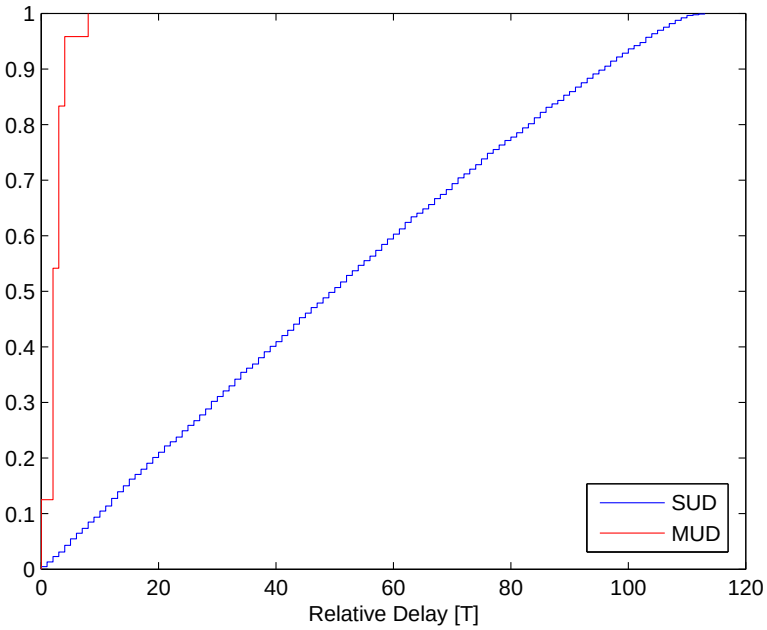

Figure 8.2: CDF of relative delays resulting in packet errors

e.g. it is more difficult when the relative channel phase and fractional delay are small. Second, we note that the MUD results are better when the first packet has a stronger power level (i.e. negative SIR). This can be explained by the inherent asymmetry of our solution. When the first packet is weaker, the acquisition and parameter estimation of the second packet are performed under noisier conditions and are less reliable.

Packet errors are more likely to occur when the overlap between the packets is longer, because then a larger part of the packet is demodulated in an interference scenario. This is demonstrated in Figure 8.2 where we show the Cumulative Distribution Function (CDF) of the relative delays for which packet errors occurred. We observe that the SUD system suffers from errors in a wider distribution of delays.

Next, we simulated the system in the presence of background noise. Table 8.2 illustrates the effect of noise level on the PER. The relative delay between the two packets was exponentially distributed with a parameter $\lambda = 0.2$. The complex channel phase was uniform, and the channel gain was fixed to maintain a SIR of 0dB. We can observe the expected degradation in performance as the background noise level increases.

E_b/N_0	SUD PER			MUD PER		
[dB]	User 1	User 2	Total	User 1	User 2	Total
30	0.1371	0.1871	0.1621	0.0013	0.0018	0.0016
27	0.1371	0.1871	0.1621	0.0023	0.0026	0.0024
24	0.1372	0.1871	0.1621	0.0047	0.0049	0.0048
21	0.1382	0.1871	0.1626	0.0104	0.0096	0.0100
18	0.1411	0.1871	0.1641	0.0251	0.0209	0.0230
15	0.1495	0.1871	0.1683	0.0518	0.0431	0.0474

Table 8.2: Packet Error Rate (PER) with different background noise levels, SIR=0 dB

Chapter 9

Conclusion and Future Work

9.1 Conclusion

In this thesis we introduced a PHY level solution to mitigate tag collisions in a transmit-only active RFID system. We exploited the MSK signal structure, which can be seen as a one-dimensional signal in a two-dimensional signal space, to jointly detect data from two tags simultaneously.

We studied two approaches for joint detection when two transmitted packets overlap. One based on joint MMSE WL demodulation, and the other nulling the signal of one of tags using projection filtering and then detecting the other. We established the superiority of the first approach and incorporated it in the final system.

Transmit-only active RFID tags generate their own clock using inexpensive hardware, and are therefore completely asynchronous. This means our system is required to estimate their frequency offsets and the relative delay between colliding packets. The wide variation in relative delays also poses some unique problems for

channel estimation. We developed an improved iterative algorithm for estimating the channel coefficients during a collision.

Finally, we demonstrated how these different algorithms work together in a full system-level simulation. We compared the performance of the MUD solution against a single user system that ignores tag collisions. As expected, we observed that our MUD design offers significant gains in performance, decreasing packet loss by an order of magnitude.

9.2 Future Work

We observed an inherent asymmetry of our design: our solution favours the case where the power level of the first packet to arrive at the receiver is higher than that of the interfering packet. The opposite case can potentially be improved by saving a buffer of samples at the receiver. If a strong interference is detected, the system can start over and detect the strong user first instead of the first to arrive.

The proposed approach cannot correctly recover a packet which collides with two other tags, even if the two interfering tags do not overlap among themselves. However, we could enhance the system to handle this case with no change to the underlying algorithms. In addition, the algorithms themselves could potentially be extended to work with multiple antennas. This would enhance the performance of the two-tag solution, as well as enable joint detection of more than two packets simultaneously.

Bibliography

[1] P. Krishna and D. Husalc. RFID infrastructure. *IEEE Communications Magazine*, 45(9):4 –10, September 2007. → pages 1

[2] IEEE 802.15 WPAN Task Group 4f (TG4f) Active RFID System. http://www.ieee802.org/15/pub/TG4f.html, 2011. [Online]. → pages 2

[3] D. Pokrajac. GuardRFID 433 MHz PHY Proposal. https://mentor.ieee.org/802.15/dcn/09/15-09-0619-00-004f-guardrfid-433-mhz-phy-proposal.ppt, 2009. [Online]. → pages 3, 4

[4] Liang Biao, Hu Ai-qun, and Qin Zhong-yuan. Trends and Brief Comments on Anti-collision Techniques in Radio Frequency Identification System. In *6th International Conference on ITS Telecommunications Proceedings*, pages 241 –245, June 2006. → pages 3

[5] J.F. Hayes and T.V.J.G. Babu. *Modeling and analysis of telecommunications networks*. Wiley-IEEE, 2004. → pages 6

[6] P.A. Murphy, M. Golanbari, G.E. Ford, and M.J. Ready. Optimum and Reduced Complexity Multiuser Detectors for Asynchronous CPM Signaling. *IEEE Transactions on Wireless Communications*, 5(8):1959 –1965, August 2006. → pages 11

[7] P. Laurent. Exact and Approximate Construction of Digital Phase Modulations by Superposition of Amplitude Modulated Pulses (AMP). *IEEE Transactions on Communications*, 34(2):150 – 160, February 1986. → pages 11

[8] B. Picinbono and P. Chevalier. Widely linear estimation with complex data. *IEEE Transactions on Signal Processing*, 43(8):2030–2033, August 1995. → pages 11, 19

[9] P. Chevalier and F. Pipon. New insights into optimal widely linear array receivers for the demodulation of BPSK, MSK, and GMSK signals corrupted by noncircular interferences-application to SAIC. *IEEE Transactions on Signal Processing*, 54(3):870 – 883, March 2006. → pages 11, 14, 19

[10] Y. Zhang, G. Bhanage, W. Trappe, Yanyong Zhang, and R. Howard. Facilitating an Active Transmit-only RFID System Through Receiver-based Processing. In *in Proceedings of the 4th Annual IEEE Communications Society Conference on Sensor, Mesh and Ad Hoc Communications and Networks*, pages 421 –430, June 2007. → pages 11

[11] D. Shen, G. Woo, D.P. Reed, A.B. Lippman, and J. Wang. Separation of multiple passive RFID signals using software defined radio. In *2009 IEEE International Conference on RFID*, pages 139–146, April 2009. → pages 12

[12] R.S. Khasgiwale, R.U. Adyanthaya, and D.W. Engels. Extracting information from tag collisions. In *2009 IEEE International Conference on RFID*, pages 131–138, April 2009. → pages

[13] C. Angerer, G. Maier, B. Delgado, M. Rupp, and J.V. Alonso. Single antenna physical layer collision recovery receivers for RFID readers. In *2010 IEEE International Conference on Industrial Technology (ICIT)*, pages 1406–1411, March 2010. → pages

[14] C. Angerer, R. Langwieser, and M. Rupp. RFID reader receivers for physical layer collision recovery. *IEEE Transactions on Communications*, 58(12):3526 –3537, December 2010. → pages 12

[15] J.G. Proakis. *Digital Communications*. McGraw-Hill, fourth edition, 2001. → pages 14

[16] U. Mengali and A.N. D'Andrea. *Synchronization techniques for digital receivers*. Springer US, 1997. → pages 17

[17] J.R. Barry, E.A. Lee, and D.G. Messerschmitt. *Digital Communication*. Springer Netherlands, 2004. → pages 22

[18] S. Ahmed, S. Lambotharan, A. Jakobsson, and J.A. Chambers. Parameter estimation and equalization techniques for communication channels with multipath and multiple frequency offsets. *IEEE Transactions on Communications*, 53(2):219 – 223, February 2005. → pages 29

[19] R. Meyer, W.H. Gerstacker, R. Schober, and J.B. Huber. A single antenna interference cancellation algorithm for increased GSM capacity. *IEEE Transactions on Wireless Communications*, 5(7):1616–1621, July 2006. → pages 30

[20] S.N. Crozier, D.D. Falconer, and S.A. Mahmoud. Least sum of squared errors (LSSE) channel estimation. In *IEE Proceedings F Radar and Signal Processing*, volume 138, pages 371–378, August 1991. → pages 41

[21] M. Bydder. Solution of a complex least squares problem with constrained phase. *Linear algebra and its applications*, 2010. → pages 43

[22] G. Lui and H. Tan. Frame synchronization for Gaussian channels. *IEEE Transactions on Communications*, 35(8):818 – 829, August 1987. → pages 50

[23] G.E. Corazza and R. Pedone. Generalized and average likelihood ratio testing for post detection integration. *IEEE Transactions on Communications*, 55(11):2159–2171, November 2007. → pages 50

[24] M.P. Fitz. Further results in the fast estimation of a single frequency. *IEEE Transactions on Communications*, 42(234):862–864, March 1994. → pages 53